The Clean Air Journal

ISSN 1017 - 1703
Vol 25 No 2
November / December 2015

Official publication of the
National Association for Clean Air

THE CLEAN AIR JOURNAL

ISSN 1017-1703
November / December 2015
Volume 25, No. 2

Published twice yearly by the National Association for Clean Air, Republic of South Africa

Website and archive copies

www.cleanairjournal.org.za

Contact

info@cleanairjournal.org.za

Contents

Guest editorial
Reflections on the Workshop on International and National Landscape of Atmospheric Mercury and the NACA Conference, 1-2 October 2015

It was a great privilege to be invited to talk at the 'Workshop on International and National Landscape of Atmospheric Mercury', and to give a presentation at this year's National Association for Clean Air Conference with the conference theme of "Shifting Challenges of Air Quality in South Africa".

The signing of the Minamata Convention on Mercury does indeed present a new challenge, not only for South Africa but for many countries around the world. While the reduction of the use of mercury in commercial and industrial products, or switching to mercury-free alternatives should be a relatively simple process, for nations such as South Africa which rely heavily on coal for power production, the reduction of mercury emissions is a significant challenge.

Mercury as an environmental cause for concern is not an issue that stands isolated from other environmental concerns; coal combustion has air quality and climate change implications as well as releasing mercury. The United Nations held its Sustainable Development Summit in the week preceding the NACA conference, and published its Sustainable Development Goals. Among these Goals is the necessity to provide "affordable, reliable, sustainable and modern energy for all". Policy makers are going to have to hard job to find a balanced approach to ensure wider energy provision while seeking to maintain a healthy environment and limit carbon emissions.

Reducing mercury emissions, however, is often a co-benefit of other measures taken to ensure reasonable air quality. The techniques used to remove sulphur and nitrogen oxides from exhaust or flue gases also reduce mercury emissions. Equally, the methods used to remove particulate matter will reduce the amount of mercury associated with particulates which is emitted.

One aspect of mercury cycling in the environment which really needs to be addressed, and particularly in the Southern Hemisphere, is that measurements are so scarce. A priority for all signatories to the Minamata convention will be the establishment of a monitoring network for mercury. Ideally, this will involve measurements of mercury in the atmosphere and in precipitation. The precipitation measurements are probably the most important, except in very polluted environments, as they provide direct evidence of the fluxes of mercury impacting rivers and reservoirs, and also agricultural and forested land. Monitoring and modelling together provide the tools necessary for a robust assessment of the environmental impact of the local and regional impact of mercury on the environment.

The NACA conference was unusual for me for one particular reason, and that was the mix of academia, government, industry and environmental consultancy representatives to be found all under one roof. And round one table. Many people helped make my stay in South Africa memorable, but special thanks must go to Prof Hannes Rautenbach, Dr Greg Feig and Bev Terry.

Ian Hedgecock
CNR Institute of Atmospheric Pollution Research

News

ARSAIO Overview: Atmospheric Research in Southern Africa and Indian Ocean: A South Africa – France bilateral collaborative programme

Venkataraman Sivakumar[1], Hassan Bencherif[2], Cathy Liousse[3], Johan Paul Beukes[4], Pieter Gideon van Zyl[4], Paola Formenti[5], Stuart Piketh[4] and Caradee Yael Wright[6]

[1] School of Chemistry and Physics, University of KwaZulu-Natal, Durban, South Africa
[2] Laboratoire de l'Atmosphère et des Cyclones, CNRS UMR 8105, Reunion University, Reunion Island, France
[3] Laboratoire d'Aérologie, CNRS UMR 5560, Toulouse, France
[4] North West University, Potchefstroom, South Africa
[5] Laboratoire Interuniversitaire des Systèmes Atmosphériques, CNRS UMR 7583
[6] South African Medical Research Council, Environment & Health Research Unit, and University of Pretoria, Department of Geography, Geoinformatics and Meteorology, Pretoria, South Africa

The "Atmospheric Research in Southern Africa and Indian Ocean" (ARSAIO) project is a research consortium of more than 25 researchers and 30 students. It is funded through a bi-lateral research programme between South Africa and France. The first phase was completed in December 2013. Now in its second phase, the project shall be completed by the end of 2017. Here, we provide an overview of the Universities/Institutes involved and French and South African co-ordinators who are investigating the structure and dynamics of the atmosphere by utilising different in-situ, space-borne and model simulation techniques.

Introduction

In the present context of global change, atmospheric and climatic research should be more organized in the framework of international collaborations and research networks. During recent years, the importance of systematic monitoring of atmospheric structure, dynamics and composition has been confirmed by satellite and ground-based observations. Together with land use change, the aerosol burden disrupts the surface/atmosphere radiative balance, as well as cloud properties, and induces regional climatic impacts. Over southern Africa, and the neighbouring oceanic regions of the Indian Ocean, these regional impacts are influenced by dynamical climate variability and play an important role in global climate change. The quantitative characterisation of these anthropogenic aerosols and their relative climatic impact is still uncertain. In this domain, the improvement and the use of integrative climate modelling tools is a necessity for environmental management and climate change mitigation (IPCC 2001, 2007). Compared to developed regions of the northern hemisphere, the tropical and austral regions of the southern hemisphere are poorly documented in terms of climate change, even though they are important components of the global atmosphere.

Scientific collaborations between French and South African laboratories started in the early 1990's with the SAFARI 1992 project dealing with the atmospheric impact of biomass burning in southern Africa. Then a long-term strong collaboration was established between French (Laboratoire d'Aérologie) and South African groups (Potchefstroom University, now called North-West University), through the IDAF (IGAC DEBITS Africa) network. Since 1994, both laboratories have been involved in the development of an African network devoted to the study of tropical atmospheric chemistry and deposition though the framework of the global programme DEBITS. This collaboration led to a cooperation programme (PICs) dealing with air pollution and climate change in South Africa called SACCLAP (Seasonal and annual trends of air quality at the South Africa scale and its impact on regional climate, health and biogeochemical cycles).

In 1997, the Laboratoire de l'Atmosphère et des Cyclones (LACy, Reunion University) and the Service d'Aéronomie (now called LATMOS) initiated a collaboration in atmospheric sciences with the University of KwaZulu-Natal (UKZN). This collaboration resulted in the implementation of a LiDAR (Light Detection and ranging) system in Durban. The Durban LIDAR was installed in 1998 - 1999, and the first operational measurements took place in 1999 (Bencherif et al., 2000). French operators and engineers travelled to Durban under the framework of a bilateral research Memorandum of Understanding to operate the system during specific campaigns (5 campaigns of several weeks each year from 1999 to 2005) and to maintain it (ten times in less than ten years). With the help of South African students and thanks to the Reunion University Student Exchange Programme, more than 20 Masters students have been able to travel to Durban to contribute to LiDAR campaigns, learn about LiDAR and other remote sensing technics, and have helped with data analysis. This cooperation has achieved nearly 400 measurement nights during the 1999-2005 period. It has resulted in one completed PhD degree, co-supervised by French and South African scientists, and several publications in peer-reviewed scientific journals.

Several cooperation projects in atmospheric research between French Centre National de le Recherche Scientifique (CNRS) laboratories and South African universities or institutes have been conducted, but they often rely on individual initiatives between two research groups. These collaborations would certainly benefit from a general collaboration framework that could be provided by an international research consortium, hence the 'Atmospheric Research in Indian Ocean and Southern Africa' (ARSAIO) project was established in 2010 by Venkataraman Sivakumar and Hassan Bencherif. The structure of the project aims to foster exchanges of scientist and students, and contribute to building important

scientific projects that could be supported by the European Union, by the French National Research Agency (ANR) or by other international institutions.

Research actions

The primary objective of the project ARSAIO (Atmospheric Research in Southern Africa and Indian Ocean) is to co-ordinate and work-together for investigating the structure and dynamics of the atmosphere by using ground-based, in-situ, space-borne and model simulation techniques. The ARSAIO research activities focus on obtaining a better understanding of southern tropics/sub-tropical areas, including:

- Atmospheric pollution and climate change in southern Africa;
- Troposphere ozone and aerosol studies over the Indian Ocean Region;
- Greenhouse gas and solar ultraviolet radiation measurements;
- Middle atmosphere dynamics and thermal structure;
- Water vapour variability in the Upper Troposphere-Lower Stratosphere (UT-LS) region; and
- Stratospheric ozone variability, transport and mixing processes in the southern tropics.

Several measurement sites around the region are involved in the project (Figure 1). The project further strengthens the research collaboration between participating French and South African partners in order to understand the aerosol and dust characteristics in the sub-tropical Southern Hemisphere. Globally, the sub-tropical Southern Hemisphere region is the least understood due to the lack of ground-based and remote sensing instruments.

The main objective of the GDRI project is to coordinate research actions and to provide a framework to build cooperative projects in response to calls for proposals from the European Union (EU), or other funding agencies.

The project involves the participation and training of Doctoral and Masters students as well as collaborations between South Africa and France. In addition to human capital development and student/research exchange between the countries, a research network exists and a number of joint research publications have been produced (see next column).

The present GDRI ARSAIO project (2nd phase) is organized into three research actions jointly managed by a French and a South African coordinator:

- Action 1: *Impact of anthropogenic pollution on southern Africa on climate change and health*
- Action 2: *Transport and deposition of mineral dust in western southern Africa*
- Action 3: *Stratosphere and troposphere interactions: ozone, water vapour, aerosols and UV radiations variability and change*

Annual workshops, conference, seminars, and training programmes are carried out to discuss research results, strengthen the research focus of the collaboration and strength student involvement in the project. To date, this has been a successful collaboration with several publications produced. A list of the most recent research articles is provided below:

- Toihir M, Bencherif H, Sivakumar V, El Amraoui L, Portafaix T, and Mbatha N. Comparison of total column ozone obtained by the IASI-MetOp satellite with ground-based and OMI satellite

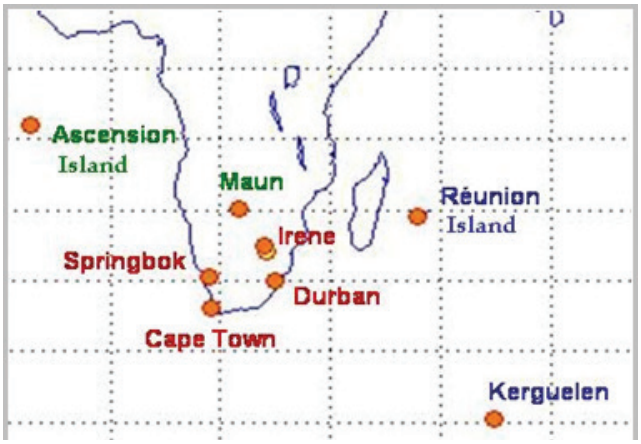

***Figure 1**: Location of French, South African and complimentary observational sites used in the framework of the GDRI ARSAIO project.*

observations in the southern tropics and subtropics, *Ann Geophys* 2015, 33: 1135–1146.

- Liousse C, Assamoi E, Criqui P, Granier C and Rosset R, African combustion emission explosive growth from 2005 to 2030, *Environ. Res Letters* 2014. DIO:10.1088/1748-9326/9/3/035003.
- Vet R, Richard S, Carou S, Shaw M, Ro C, Aas W, Baker A, Bowersox VC, Dentener F, Galy-Lacaux C, Hou A, Pienaar JP, Gillett R, Forti MC, Gromov S, Hara H, et al. A global assessment of precipitation chemistry and deposition of sulfur, nitrogen, sea salt, base cations, organic acids, acidity and pH, and phosphorus. *Atmospheric Environment* 2014, 93: 3-100.
- Olakunle O, Sivakumar V and Mbatha N. A case study of energy deposition and absorption by magnetic cloud electrons and protons over the high latitude stations effects on mesosphere and lower thermosphere, J. Terr. *Atmos and Oceanic Sciences* 2014, 25(2): 219-232.

Acknowledgements

The ARSAIO project is supported by the French Centre National de la Recherche Scientifique (CNRS) and the South African National Research Foundation (NRF-UID 78682). Authors acknowledge the CNRS and NRF for their continuous financial support.

References

Bencherif H, Morel B, Moorgawa A, et al., 2000, First validation of stratospheric temperature profiles obtained by a Rayleigh LIDAR over Durban, South Africa. *South African J. of Sci*., 96:487–492., 2000.

IPCC, 2001, *Third Assessment Report of the Intergovernmental Panel on Climate Change: Mitigation*.

IPCC, 2007, *Fourth Assessment Report of the Intergovernmental Panel on Climate Change: Mitigation and Climate Change*.

Highlighted local research
Mercury measurements at Cape Point, South Africa – an update on recent findings

Brunke, E-G., Walters, C., Mkololo, T., Martin, L., Labuschagne, C., Silwana, B., Slemr, F., Weigelt, A., Ebinghaus, R. and Somerset, V

Mercury (Hg) is regarded as a highly toxic, heavy metal and is also considered as a global pollutant due to its long range transport and bio-accumulation in the aquatic nutrition chain, which is not fully understood yet. For this reason and also to initiate international legislation aimed at controlling the use of mercury, a European Union-funded Global Mercury Observing System (GMOS), in which the Cape Point Global Atmospheric Watch (GAW) station participated, was initiated in 2010. The South African Weather Service (SAWS) as well as the Council for Scientific and Industrial Research (CSIR) have been conducting mercury measurements at the Cape Point GAW station since 1995 and 2007, respectively. While SAWS focussed on the measurement of Gaseous Elemental Mercury (GEM) in air, the CSIR has carried out analyses of Total mercury (TotHg) in precipitation samples. The GEM measuring programme, which is ongoing, has led to several publications dealing with long-term trends, seasonal cycles, depletion events and continental emission estimates for Hg.

In a recent study (Brunke et al., 2015) - briefly summarized here - a comparison between these two Hg species (i.e. GEM and TotHg) is made over a seven year period (2007-2013) using the results obtained during the rainy season (May – October). This study represents a follow-up (with new findings) to an initial investigation conducted by Gichuki and Mason (2013) which comprised a much smaller data set.

Rain events experienced at Cape Point are almost exclusively linked to cold fronts from the Atlantic Ocean. For the 2007 - 2013 period, 75% of all air mass trajectories coupled to these rain episodes reached the Cape Point GAW station directly from the southern ocean, while 19% arrived there with a short bypass over the Cape Town metropolitan area. Merely 6% approached Cape Point along the sea from the East via the Cape Agulhas sub-continental region. The atmospheric levels of carbon monoxide (CO) and ^{222}Rn (a tracer for marine air) in the 85 rain events identified are largely characteristic of maritime conditions. Although a few rain fronts which had passed over the greater Cape Town area before arriving at Cape Point from the North - sometimes revealed slightly elevated CO and ^{222}Rn levels, no statistically significant local anthropogenic influences were detected in the GEM and TotHg data. Over the 2007 - 2013 period, the May to October averages for GEM ranged from 0.913 ng m^{-3} to 1.108 ng m^{-3}, while TotHg concentrations ranged from 0.03 to 52.5 ng L^{-1} (overall average: 9.91 ng L^{-1}).

A close coupling has been found to exist between GEM and TotHg (2007-2014). The average GEM levels for the wet season show a positive correlation (R^2 = 0.49; n=7) with TotHg. Furthermore, both GEM and TotHg display similar, relative inter-annual concentration variations over the measuring period as a function of rain depth (not shown here, see published article).

The most noteworthy result, however, is the strong correlation observed between GEM and the El-Niño Southern Oscillation (ENSO) signal, especially during the 1996 - 2004 period (Figure 1).

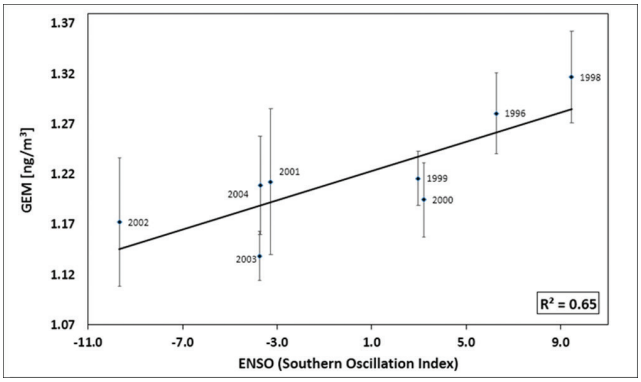

***Figure 1**: Relationship between GEM averages (May to October) and Southern Oscillation Index (SOI, http://www.bom.gov.au/climate/current/soi2.shtml): 1996 - 2004. The error bars represent GEM standard deviations. Linear regression: GEM = 0.007*SOI + 1.216 [taken from Brunke et al., 2015].*

These correlations (Figure 1) suggest that the inter-annual variations of GEM (and also TotHg) concentrations are primarily influenced by large scale weather phenomena. Meteorological processes can affect mercury emissions directly, for example, by periodic changes of surface ocean temperatures during ENSO events, or indirectly via extended droughts leading to increased biomass burning which in many cases is also a source of GEM. These processes can also influence the oxidation of GEM to species prone to rain and washout as has been reported elsewhere. However, changing oxidation rates would influence TotHg concentrations to a substantially larger degree than those of GEM, and would, at constant emissions, lead to an anti-correlation between GEM and TotHg concentrations and this is not observed.

We thus conclude that meteorological influences on mercury emissions is the major reason for the positive GEM versus TotHg and GEM versus SOI correlations. The SOI influence on tropospheric mercury concentrations has since been further investigated – also for the Northern Hemisphere in an unpublished study (currently under review) by Slemr et al. ("El-Niño Southern Oscillation (ENSO) influence on tropospheric mercury concentrations").

References

Brunke E-G, Walters C, Mkololo T, Martin L, Labuschagne C, Silwana, B, Slemr F, Weigelt A, Ebinghaus R and Somerset V. Mercury in the atmosphere and in rainwater at Cape Point, South Africa. *Atmospheric Environment 2015*, DOI:10.1016/j.atmosenv.2015.10.059.

Gichuki SW and Mason RP. Mercury and metals in South African precipitation. *Atmospheric Environment 2013*, 79: 286-298.

Research brief
Recent papers utilizing Cape Point mercury monitoring data

Mercury is a globally important toxin that has the potential to cause significant adverse impacts to human and environmental health. Mercury that is released from natural or anthropogenic activities has the ability to enter the atmosphere and due to its long atmospheric lifespan it is able to be transported great distances around the world. As part of the biogeochemical cycling of mercury, gaseous elemental mercury (GEM) (the most abundant species of atmospheric mercury, accounting for >90% of the total atmospheric mercury) is able to be oxidised and is deposited in water and on land, where it undergoes further biogeochemical cycling to form methylated mercury.

The methylated mercury is biologically active and is able to enter the tissue of plants and animals and is potentially bio-accumulated and concentrated at higher trophic levels. It is particularly problematic in large piscivorous fish and marine mammals, which if consumed regularly can be a source of mercury toxicity for human populations. Globally, there are a number of sites that continuously monitor background concentrations of atmospheric mercury. Most of these sites are located in the Northern Hemisphere, however, there is one site in South Africa, located at the Cape Point Global Atmospheric Watch (GAW) station that has a near continuous monitoring record dating back to 1995.

The Cape Point GAW station is equipped with a Tekran 2537A vapour-phase mercury analyser resolution (Tekran Inc, Toronto Canada), set to a 15 minute temporal. The analyser has total gaseous mercury detection limit of ~0.05 ng/m^3. It is thought that under the conditions at the Cape Point station, only GEM will be measured since the inlet manifold has a 30m high inlet with PTFE tubing, a PTFE filter and the presence of sea salt aerosols that is expected to trap the other mercury species. In addition to the mercury measurements the Cape Point GAW station measures carbon dioxide (CO_2), carbon monoxide (CO), methane (CH_4), ozone (O_3), nitrous oxide (N_2O) and halocarbons.

Several articles published in the international scientific literature use the atmospheric mercury record from the GAW Cape point station, emphasising once again the international importance of this site. A paper titled '**Comparison of mercury concentrations measured at several sites in the Southern Hemisphere**" was published written by Franz Slemr and others in Atmospheric Chemistry and Physics (Slemr et al., 2015). The authors used data from four remote monitoring stations located at Amsterdam Island (southern Indian Ocean between southern Africa and Australia), Cape Grim (Tasmania), Cape Point (South Africa) and Troll Research Station (Antarctica). They compare the monthly and annual average and median concentrations of the measurements taken at the four remote southern hemisphere stations. The Cape Point and Amsterdam Island Stations showed no significant differences in terms of the monthly mean values and both showed that there was no discernible seasonal variation. The Troll station in Antarctica showed significant seasonal variation with peaks in mercury concentrations in the months of February and March and a minimum during October - December. The Cape Grim data showed the greatest seasonal variation and a large and random scatter of the monthly median values, indicating that the data are not as homogenous as the other sites. Median monthly values for all the stations ranged from ~0.8- 1.1 ng/m^3. On an annual basis, the medians of the annual mercury gradients were small and did not exceed 0.2ng/m^3. However, at the Cape Point station an increasing trend in the mercury concentration was observed for the period 2007 to 2013, compared to a decreasing trend in the mercury concentrations between 1996 and 2004.

The second article is titled "**Statistical exploration of gaseous elemental mercury (GEM) measured at Cape Point from 2007 to 2011**" was by Andrew Venter and others (Venter et al., 2015). The paper had two main focal areas, namely 1) back trajectory analysis to improve the understanding of the source regions of GEM recorded at Cape Point, and 2) the development of a multiple linear regression model to predict the concentrations of GEM at Cape Point from the other parameters measured from monitored data for the period March 2007 to December 2011. The back trajectory analysis showed that the data could be represented in two main clusters with a separation at a GEM concentration of 0.904ng/m^3. The lower GEM concentration air masses have source regions that pass over the sparsely populated interior of South Africa and the remote marine regions, while the higher GEM concentration cluster is associated with air masses that originate along the shipping lanes that skirt the South African coast and the coastal cities.

The second part of the study used a process of multiple linear regressions to model the concentrations of GEM. The linear model included eight terms which showed either a positive or negative impact on the GEM concentrations. The terms that showed a positive correlation with the GEM concentration included absolute humidity, CO concentration, atmospheric pressure, temperature and methane concentration. The terms that showed a negative correlation with the GEM included ozone concentration, radon concentration and wind gust speed. When the monitored and predicted results are considered the fitted slope of the linear regression indicates a slight decreasing trend in the GEM concentrations for the period 2007-2011. This is in contrast to the increase observed in the 2007 - 2013 dataset discussed in the Slemr et al. (2015) paper. The authors suggest that the differences in the trends reported in these two studies are a result of differences in the data validation and processing procedures that were applied.

References

Slemr, F, H Angot, a Dommergue, O Magand, M Barret, a Weigelt, R Ebinghaus, et al. 2015. "Comparison of Mercury Concentrations Measured at Several Sites in the Southern Hemisphere." *Atmospheric Chemistry and Physics* 15 (2011): 3125–3133. doi:10.5194/acp-15-3125-2015.

Venter, a. D., J. P. Beukes, P. G. van Zyl, E.-G. Brunke, C. Labuschagne, F. Slemr, R. Ebinghaus, and H. Kock. 2015. "Statistical Exploration of Gaseous Elemental Mercury (GEM) Measured at Cape Point from 2007 to 2011." *Atmospheric Chemistry and Physics* 15 (18): 10271–10280. doi:10.5194/acp-15-10271-2015. http://www.atmos-chem-phys.net/15/10271/2015/.

Commentary
Mercury Emissions in South Africa
Perspective from the Department of Environmental Affairs

Vincent Gololo
Climate Change and Air Quality, Department of Environmental Affairs

Introduction

The Department of Environmental Affairs (DEA) recognises the need to protect human health and the environment from anthropogenic emissions of mercury. In 2003, various governments agreed on the need for global action on mercury based on its adverse health and environmental effects. Later, in 2009, they negotiated a legally-binding instrument on mercury and established the Intergovernmental Negotiating Committee (INC). Five INC negotiation sessions were held and in January 2013, the negotiations were finalised. The content of the convention, known as the Minamata convention, was adopted in October 2013 in Minamata, Japan and South Africa was a signatory of the convention.

South Africa enacted the Air Quality Act (NEM:AQA) and Waste Management Act (NEM:WMA) which provide for the enforcement of mercury emission limits, regulating mercury pollution, mercury storage, rehabilitation of contaminated sites, as well as the responsible management and disposal of mercury waste. Listed activities under NEM:AQA (Act No 39 of 2004) with mercury emission limits are waste co-feeding combustion installations (Subcategory 1.6), production and processing of zinc, nickel and cadmium (Subcategory 4.14), metal recovery (Subcategory 4.23), cement production (using alternative fuels and/or resources) (Subcategory 5.5), lime production (using alternative fuels and/or resources) (Subcategory 5.7), thermal treatment of general waste (Subcategory 8.1) and drum recycling processes (Subcategory 8.4).

Mercury Emissions Inventory in South Africa

Previous estimates of South Africa's anthropogenic mercury emissions were 256.7 tons in 2000 (Pacyna et al. 2003, Pacyna et al. 2006). The report considered coal combustion and gold mining as the most significant sources. Based on this estimate, South Africa was ranked as the second highest emitter of mercury in the world, accounting for 16% of global anthropogenic emissions. These findingsprompted further local studies and the establishment of the South African Mercury Assessment (Leaner et al. 2009).

The DEA completed work funded by the United Nations Environment Program (UNEP) on mercury emissions in 2011. The work focused on mercury emissions from coal-fired power stations. The total mercury emissions from coal-fired power stations for 2009 - 2010 was estimated to be 39.4 tons per annum. This was comparable with other studies (Leaner et al. 2009, Masekoameng et al. 2010). A level 1 inventory study was also undertaken in 2011 and a level 2 study is intended to do a detailed inventory using the UNEP Toolkit Level 2. The DEA is in the process of conducting the level 2 inventory study which will improve the accuracy of the data obtained from level 1 study. The introduction of the National Atmospheric Emissions Inventory System (NAEIS) will also assist in building a detailed mercury emission inventory in the country.

Conclusion

The integration of mercury into the national environmental agenda in South Africa requires accurate and detailed sector-based mercury inventory studies. These will add a component on cost-benefit analysis to gauge the socio-economic implications for South Africa if it ratifies the Minamata Convention on mercury for all affected sectors and industries.

References

Leaner J.J., Dabrowski J.M., Mason R.P., Resane T., Richardson M., Ginster M., Gericke G., Petersen C.R., Masekoameng E., Ashton P.J and Murray K., 2009.,Mercury Emissions from Point Sources in South Africa. In *Mercury Fate and Transport in the Global Atmosphere*, Eds: N. Pirrone and R. Mason, Springer Science and Business Media.

Masekoameng E., Leaner J.J. and Dabrowski J.A., 2010. Trends in anthropogenic mercury emissions estimated for South Africa during 2000 to 2006, *Atmospheric Environment*, 44, 3007 – 3014.

Pacyna J.M., Pacyna E.G., Steenhuisen F. and Wilson S., 2003. Mapping 1995 global anthropogenic emissions of mercury, *Atmospheric Environment*, 37, 109 – 117.

Pacyna E.G., Pacyna J.M., Steenhuisen F. and Wilson S., 2006. Global anthropogenic mercury emission inventory for 2000, *Atmospheric Environment*, 40, 4048 – 4063.

Commentary
Perspectives on South African atmospheric mercury scientific research

Patricia Forbes
Department of Chemistry, University of Pretoria, Pretoria

On the 30 September 2015, a workshop entitled "International and National Landscape of Atmospheric Mercury" was held in Bloemfontein prior to the start of the annual National Association for Clean Air (NACA) Conference. Dr Ian Hedgecock of the CNR-Institute of Atmospheric Pollution Research in Italy provided a global context to atmospheric mercury levels, impacts and policy and highlighted challenges faced (see his commentary for more information), whilst Dr Vincent Gololo of the Department of Environmental Affairs provided a summary of the status of the development of the South African mercury emissions inventory.

Several researchers from the South African air quality community then presented work their work in the field of atmospheric mercury, which is briefly summarised here. Dr Pieter van Zyl of the Unit of Environmental Sciences and Management at the North-West University discussed the statistical analysis of the gaseous elemental mercury (GEM) monitoring data from the Global Atmospheric Watch (GAW) station at Cape Point, from which predictive/estimation equations were developed. Shipping trade routes were identified as a potential source of atmospheric Hg and a decline in GEM at the site over the period evaluated was noted (Venter et al., 2015).

Dr Patricia Forbes gave an overview of analytical chemistry research in atmospheric mercury monitoring, which had largely been undertaken at the Council for Scientific and Industrial Research (CSIR). The use of cost-effective, portable, alternative Hg monitoring methods were discussed; namely sorbent tube sampling and biomonitoring (using lichens as passive samplers) were compared to a semi-continuous mercury analyser (Trüe et al., 2010 and 2012). These alternative methods can be used to identify "hotspots" to guide the placement of more comprehensive, expensive monitoring equipment.

Dr Lynwill Martin of the South African Weather Service provided detail regarding the 19 years of monitoring of gaseous elemental mercury at the Cape Point GAW station. The first paper on the results obtained was published in 2002 (Baker et al., 2002), which noted a 12 month lag period between Hg levels in the Northern and Southern Hemispheres. Following from the installation of a Tekran instrument in 2007, unique mercury depletion events were noted at the site, where Hg levels decrease to less than 75% of normal background levels and which last for longer than 4 hours and are not accompanied by a decrease in ozone (Brunke et al., 2010). This phenomenon has generated a significant amount of interest from the international scientific community. Positive correlations have also been found between mercury concentrations in the atmosphere (GEM) and rainwater (total mercury) at Cape Point over a seven year period (2007-2013) (Brunke et al., 2015) (see the Research Brief by Brunke et al. for more details).

Prof Hannes Rautenbach of the Laboratory for Atmospheric Studies at the University of Pretoria gave an overview of the atmospheric mercury dispersion and deposition distribution modelling that is being undertaken using the Weather Research and Forecasting (WRF) model and fine resolution (3 km).

Future collaborations and projects planned were also mentioned by presenters, which indicates that interest in this field is continuing, and that further contributions to the science of atmospheric mercury are expected to be made by South African air quality researchers in the future.

References

Baker, P.G.L., Brunke, E.-G., Slemr, F. and Crouch, A.M., 2002, Atmospheric mercury measurements at Cape Point, South Africa, *Atmospheric Environment*, 36(14): 2459-2465.

Brunke, E.-G., Labuschagne, C, Ebinghaus, R., Kock, H.H. and Slemr, F., 2010, Gaseous elemental mercury depletion events observed at Cape Point during 2007-2008, *Atmospheric Chemistry and Physics*, 10: 1121-1131.

Brunke, E.-G., Walters, C., Mkololo, T., Martin, L., Labuschagne, C., Silwana, B., Slemr, F., Weigelt, A., Ebinghaus, R. and Somerset, V., 2015, Mercury in the atmosphere and in rainwater at Cape Point, South Africa, *Atmospheric Environment*, DOI: 10.1016/j.atmosenv.2015.10.059.

Trüe, P. Forbes, N. Panichev and J. Okonkwo, 2010, The use of sorbent tubes and a semi-continuous emissions monitor for the determination of atmospheric total gaseous mercury in Pretoria, South Africa, *Fresenius Environmental Bulletin*, 19 (12a): 3007-3012.

Trüe, N. Panichev, J. Okonkwo and P.B.C. Forbes, 2012, Determination of the mercury content of lichens and comparison to atmospheric mercury levels in the South African Highveld Region, *The Clean Air Journal*, 21 (1): 19-25.

Venter, A.D., Beukes, J.P., van Zyl, P.G., Brunke, E.-G., Labuschagne, C., Slemr, F., Ebinghaus, R. and Kock H., 2015, Statistical exploration of gaseous elemental mercury (GEM) measured at Cape Point from 2007 to 2011, *Atmos. Chem. Phys. Discuss.*, 15: 4025-4053.

Commentary
Emission accomplished: formal and informal mercury sources in South Africa

Renée A. Street
Environment & Health Research Unit, South African Medical Research Council and Discipline of Occupational and Environmental Health, University of KwaZulu-Natal

Mercury (Hg) is a naturally occurring element that is present in air, water and soil. It exists in three main forms namely elemental mercury, inorganic mercury compounds and organic mercury compounds (WHO, 2007). The atmosphere is the leading transport pathway of mercury emissions, while land and ocean processes maintain a central role in mercury redistribution among terrestrial, marine and freshwater ecosystems (Driscoll et al., 2013). The biogeochemical cycling of mercury is complex, comprising various transport and transformation progressions that define the fate of mercury and the health risks on ecosystem and humans (Liu et al., 2011).

Mercury is an obstinate pollutant that bio-accumulates and biomagnifies across trophic levels (Kidd et al., 2012). Akin to only a few metal elements, it amasses through food webs to quantities that are conspicuously higher in upper trophic level organisms compared with primary producers or consumers (Kidd et al., 2012). Numerous pathways exist for human mercury exposure including through air, food, water, pharmaceuticals and cosmetics (Williams et al., 2011). The form of mercury determines the route of exposure, absorption, distribution and target organ toxicity (Park and Zheng, 2012) and human exposure to mercury can result in numerous acute and chronic manifestations including neurological problems (Bose-O'Reilly et al., 2010; Schmidt, 2012). Methylmercury, which passes more readily into the brain, is commonly considered the more toxic species, predominantly among children (Schmidt, 2012; Zillioux, 2015). Consumption of methylmercury-contaminated fish is the main route of exposure to organic mercury (Holmes et al., 2009). Conversely, this poses a public health challenge because fish are highly nutritious with substantial health benefits (Mergler et al., 2007). Furthermore, fish are culturally important for many societies and create an essential global commodity (Mergler et al., 2007).

Currently, anthropological activities account for approximately 30% of the total mercury entering the atmosphere annually (UNEP, 2013). In 2001, the United Nations Environmental Programme (UNEP) commissioned a global assessment of mercury in response to mounting concern regarding mercury emissions as well as unremitting mercury poisoning incidence reports (Dabrowski et al., 2008; DEA, 2011). The assessment, in the form of country-specific inventories, quantifies mercury emissions from several sources (Dabrowski et al., 2008). The most recent global mercury inventory has identified the role of artisanal and small-scale gold mining (ASGM) and coal burning as the largest constituents of anthropogenic emissions, tailed by the production of ferrous and non-ferrous metals, and cement production (UNEP, 2013). In a global response to phase out mercury, the Minamata Convention on Mercury was adopted in Japan in October 2013. Minamata disease is caused by mercury toxicity and results in extreme neurological damage (Larson, 2013). Hence the name and locality of the Convention is indeed apt in memory of the first case of Minamata disease identified nearly six decades earlier (Sharma, 2014). According to Selin (2014), the Convention is a key addition to the patchy treaty landscape on hazardous substances.

In keeping with global trends and efforts, high quality, continuous mercury monitoring is now underway in South Africa (UNEP 2013). Global patterns have identified South Africa among the countries with the highest levels of elemental mercury in the air (UNEP 2013). The South African mercury inventory, completed in 2011, flagged the key anthropogenic mercury sources as coal combustion, crude oil, ferrous and non-ferrous metals, artisanal mining and consumer products. In response to high mercury emissions from coal combustion, South Africa has recently made inroads into mercury characterization of coal and coal combustion products. This will inform best practices regarding air pollution control devices and/or coal-washing (Kolker et al., 2014). Unintentional mercury emissions from similar sectors such as mining, smelting, and production of iron and non-ferrous metals, cement product and oil refining can also be reduced with the use of pollution control measures at power stations and industrial plants (UNEP, 2013). However, this will depend on scientific aptitude and political will, both of which are complex and interrelated (Selin 2005).

Arguably, the more challenging mercury exposure sources to tackle are those from the informal sectors. South African examples include (but are not limited to) illegal mining operations, socio-cultural and ritualistic practices and the use of prohibited cosmetics. The poverty-driven ASGM industry is on the increase in many low- and middle income countries largely due to the rising gold price (Basu et al., 2015). Elemental mercury is used to extract gold from ore by forming "amalgam", a mixture comprising roughly one part mercury to one part gold (Gibb and O'Leary, 2014). Despite the fact that the miners and those involved in the trade may be exposed to dangerous levels of elemental mercury vapour, data on health outcomes are scarce and little is known about linkage to healthcare (Gibb and O'Leary, 2014; Basu et al., 2015). With an association of

illegality, 'Zama-Zama' is the colloquial South African name for 'artisanal' gold miners (Nhlengetwa and Hein, 2015). According to the Chamber of Mines (2015), the value of illegal gold mining is up to 10% of annual South African gold production which in 2013 was over R72 billion. However, in line with the global trend, the occupational and environmental hazards associated with the informal ASGM trade in South Africa remain largely undocumented.

In order to reduce mercury-related diseases, the World Health Organization (WHO) has accentuated the need to identify traditional practices involving mercury. Up until recently, socio-cultural use of mercury in South Africa was merely anecdotal. So much so, that in the South African mercury inventory the response to the question on mercury use in traditional medicine was that the practice is non-existent (DEA, 2011). However, newly published research on mercury use in South African traditional medicine revealed that 39% (n=78) of traditional health practitioners (THPs) stated that they administer mercury (*isigidi*) for healing purposes (Street et al., 2015). Moreover, this finding is cumulative with 95% of the mercury-using THPs stating that they learnt how to use it from companion THPs (Street et al., 2015). This is of concern in a country with approximately 27 million consumers of traditional medicine (Mander et al., 2007).

A third example of a locally-threatening mercury source is that of the cosmetics industry's informal sector. Mercury is a common ingredient found in skin lightening products in the form of creams and soaps (WHO, 2011). Mercury-containing skin lightening cosmetics are available locally to meet the demands of the South African population (Dlova et al., 2012). A recent cross-sectional study revealed that from six hundred African and Indian women residing in South Africa, 33% used skin lightening products (Dlova et al., 2015). Hence, according to the South African mercury inventory of 2011, women using skin lightening creams and soaps have been identified as vulnerable populations. Stronger regulations and restrictions need to be imposed on readily accessible cosmetics (Dlova et al. 2012), especially those available at informal trading sites.

Despite having identified potential sources of mercury, the extent of mercury exposure in local South African communities remains largely unknown (Oosthuizen et al., 2010). Much directed and interdisciplinary work is needed in order to document, regulate and remedy the locally-relevant mercury-emitting activities. Nonetheless, each implemented change is bound to have its own repercussions, with 'one risk traded for another' (Larson, 2013). In South Africa, community mobilization is vital in order to reach the ultimate goal, namely to protect human health and the environment from the adverse effects of mercury.

References

Basu, N., Clarke, E., Green, A., Calys-Tagoe, B., Chan, L., Dzodzomenyo, M., Fobil, J., Long, R. N., Neitzel, R. L., and Obiri, S. 2015. Integrated Assessment of Artisanal and Small-Scale Gold Mining in Ghana—Part 1: Human Health Review. *Int. J. Environ. Res. Public Health*, 12, 5143-5176.

Bose-O'Reilly, S., McCarty, K. M., Steckling, N., and Lettmeier, B. 2010. Mercury exposure and children's health. *Curr. Probl. Pediatr. Adolesc. Health Care*, 40, 186-215.

Chamber of Mines of South Africa. 2015. Illegal Mining in South Africa. Fact sheet 2015., Johannesburg.

Dabrowski, J. M., Ashton, P. J., Murray, K., Leaner, J. J., and Mason, R. P. 2008. Anthropogenic mercury emissions in South Africa: Coal combustion in power plants. *Atmospheric Environment*, 42, 6620-6626.

DEA. 2011. Inventory of mercury releases in South Africa. Pretoria.

Dlova, N., Hamed, S., Tsoka-Gwegweni, J., and Grobler, A. 2015. Skin lightening practices: an epidemiological study of South African women of African and Indian ancestries. *Br. J. Dermatol*., 173, 2-9.

Dlova, N. C., Hendricks, N. E., and Martincgh, B. S. 2012. Skin-lightening creams used in Durban, South Africa. *Int. J. dermatol*., 51, 51-53.

Driscoll, C. T., Mason, R. P., Chan, H. M., Jacob, D. J., and Pirrone, N. 2013. Mercury as a global pollutant: sources, pathways, and effects. *Environ. Sci. Technol*., 47, 4967-4983.

Gibb, H., and O'Leary, K. G. 2014. Mercury exposure and health impacts among individuals in the artisanal and small-scale gold mining community: a comprehensive review. *Environ. Health Perspect*., 122, 667.

Holmes, P., James, K. A. F., and Levy, L. S. 2009. Is low-level environmental mercury exposure of concern to human health? *Sci. Total Environ*., 408, 171-182.

Kidd, K., Clayden, M., and Jardine, T. 2012. Bioaccumulation and biomagnification of mercury through food webs. Pages 455-499 *Environmental chemistry and toxicology of mercury*., Wiley, Hoboken.

Kolker, A., Senior, C. L., and van Alphen, C. 2014. Collaborative studies for mercury characterization in coal and coal combustion products, Republic of South Africa. 2331-1258, US Geological Survey.

Larson, H. J. 2013. The Minamata Convention on Mercury: risk in perspective. Lancet, 383, 198-199.

Liu, G., Cai, Y., O'Driscoll, N., Feng, X., and Jiang, G. 2011. Overview of mercury in the environment. Pages 1-12 Environmental chemistry and toxicology of mercury.

Mander, M., Ntuli, L., Diederichs, N., and Mavundla, K. 2007. Economics of the traditional medicine trade in South Africa:

health care delivery. *South African health review*, 189-196.

Mergler, D., Anderson, H. A., Chan, L. H. M., Mahaffey, K. R., Murray, M., Sakamoto, M., and Stern, A. H. 2007. Methylmercury exposure and health effects in humans: a worldwide concern. *AMBIO: A Journal of the Human Environment*, 36, 3-11.

Nhlengetwa, K., and Hein, K. A. 2015. Zama-Zama mining in the Durban Deep/Roodepoort area of Johannesburg, South Africa: An invasive or alternative livelihood? *The Extractive Industries and Society*, 2, 1-3.

Oosthuizen, M., John, J., and Somerset, V. 2010. Mercury exposure in a low-income community in South Africa. *S. Afr. Med. J.*, 100, 366-371.

Park, J.-D., and Zheng, W. 2012. Human exposure and health effects of inorganic and elemental mercury. *J. Prev. Med. Public Health*, 45, 344.

Schmidt, C. W. 2012. Quicksilver & gold. Environ. *Health Perspect*, 120, 424-429.

Selin, H. 2014. Global environmental law and treaty-making on hazardous substances: the Minamata Convention and mercury abatement. *Global Environmental Politics*, 14, 1-19.

Selin, N. E. 2005. Mercury rising: Is global action needed to protect human health and the environment? *Environment: Science and Policy for Sustainable Development*, 47, 22-35.

Sharma, A. 2014. Legally binding Minamata Convention on Mercury: politics and science behind. *Curr. Sci.*, 106, 1063.

Street, R. A., Kabera, G. M., and Connolly, C. 2015. Metallic mercury use by South African traditional health practitioners: perceptions and practices. *Environ. Health*, 14, 67.

UNEP. 2013. Global Mercury Assessment 2013: Sources, Emissions, Releases and Environmental Transport. *UNEP Chemicals Branch Geneva*, Switzerland.

WHO. 2007. Exposure to mercury: A major public health concern., Geneva.

WHO. 2011. Preventing disease through healthy environments: mercury in skin lightening products., Geneva.

Williams, C. R., Leaner, J. J., Somerset, V. S., and Nel, J. M. 2011. Mercury concentrations at a historically mercury-contaminated site in KwaZulu-Natal (South Africa). *Environ. Sci. Pollut. Res.*, 18, 1079-1089.

Zillioux, E. J. 2015. Mercury in Fish: History, Sources, Pathways, Effects, and Indicator Usage. Pages 743-766 *Environmental Indicators*. Springer.

Indoor and outdoor particulate matter concentrations on the Mpumalanga highveld – A case study

Bianca Wernecke*[1] Brigitte Language[1], Stuart J. Piketh[1] and Roelof P. Burger[1]
*Eskom Holdings SOC Ltd, Megawatt Park, Maxwell Drive, Sunninghill, 2001
[1] Unit for Environmental Sciences and Management, North West University, Potchefstroom, 2520, South Africa, wernecb@eskom.co.za, bl23034149@gmail.com, Stuart.Piketh@nwu.ac.za, Roelof.Burger@nwu.ac.za

Received: 20 October 2015 - **Reviewed:** 6 November 2015 - **Accepted:** 17 November 2015
http://dx.doi.org/10.17159/2410-972X/2015/v25n2a1

Abstract
The household combustion of solid fuels, for the purpose of heating and cooking, is an activity practiced by many people in South Africa. Air pollution caused by the combustion of solid fuels in households has a significant influence on public health. People most affected are those considered to be the poorest, living in low-income settlements, where burning solid fuel is the primary source of energy. Insufficient data has been collected in South Africa to quantify the concentrations of particulate emissions that people are exposed to, especially the respirable fraction, associated with the combustion of solid fuels. The aim of this paper is to gain an understanding of the particulate matter (PM) concentrations a person living in a typical household in a low income settlement in the South African Highveld is exposed to. It also seeks to demonstrate that the use of solid fuels in the household can lead to indoor air pollution concentrations reaching levels very similar to ambient PM concentrations, which could be well in excess of the National Ambient Air Quality Standards, representing a major national public health threat. A mobile monitoring station was used in KwaDela, Mpumalanga to measure both ambient particulate concentrations and meteorological conditions, while a range of dust/particulate monitors were used for indoor and personal particulate concentration measurements. Indoor and personal measurements are limited to the respirable fraction (PM_4) as this fraction contributes significantly to the negative health impacts. The sampling for this case study took place from 7-19 August 2014. Highest particulate matter concentrations were evident during the early mornings and the early evenings, when solid fuel burning activities were at their highest. Indoor and personal daily average PM_4 concentrations did not exceed the 24h National Ambient $PM_{2.5}$ Standard of 65 µg/m^3 nor did they exceed the 24h National Ambient PM_{10} Standard of 75 µg/m^3. The outdoor $PM_{2.5}$ concentrations were found to be below the standards for the duration of the sampling period. The outdoor PM_{10} concentrations exceeded the standards for one day during the sampling period. Results indicate that, although people in KwaDela may be exposed to ambient PM concentrations that can be non-compliant to ambient standards, the exposure to indoor air, where solid fuel is burnt, may be detrimental to their health.

Keywords
particulate matter exposure, indoor air quality, ambient air quality, personal exposure

Introduction
The household combustion of solid fuels (coal, wood, dung, and crop waste), for the purpose of heating and cooking, is an activity practiced by approximately 3 billion people around the world (Chafe et al. 2014). Air pollution caused by the combustion of these solid fuels has a significant influence on public health, attributing to more than 4 million premature deaths globally in 2012 (Bruce et al., 2015). People most affected are those living in low- income settlements in developing countries, where burning solid fuels is the primary source of domestic energy (Xie et al. 2015).

In South Africa, the low level burning of solid fuels such as coal and wood contributes significantly to the high levels of ambient air pollution in the country (Terblanche et al. 1992).Many people in rural communities and in townships utilise solid fuels for cooking and heating. Exposure to the emissions, in particular to the respirable aerosols stemming from these burning practices is known to cause a large number of health problems (Smith 2000). Various literature sources have acknowledged that ambient pollution levels are not necessarily indicative of the concentrations of air pollution that humans are exposed to on an everyday basis, as most people tend to spend most of their time indoors (Lim et al. 2012, Diapouli et al. 2011, Ferro et al. 2004, Smith 2002). The Medical Research Council Burden of Disease Research Unit ranked indoor air pollution at number 15 for South Africa, higher than urban air pollution (MRC 2008, Norman et al. 2007).

This paper aims to evaluate the level of indoor and outdoor

particulate matter exposure within a typical household in a low-income settlement in Mpumalanga, South Africa (KwaDela) in the winter period, the time of year in which low level burning practices are particularly prevalent, and to demonstrate that the use of solid fuels in the household level can lead to indoor air pollution concentrations reaching well in excess of the National Ambient Air Quality Standards, representing a major national public health threat.

The following questions were answered (i) what is the outdoor, indoor, and personal exposure of residents; (ii) what is the relationship between outdoor, indoor and personal mass concentration measurements; and (iii) what are the associated diurnal patterns of exposure of residents during the sampling period.

Experimental Method

Sampling Site

KwaDela (26°27'47.53"S; 29°39'51.73"E) is situated in the Gert Sibande Disctrict Municipality of Mpumalanga, South Africa, which lies in the Highveld Priority Area. Located approximately 200 km South-East of Johannesburg. According to census data, Kwadela has a population of about 3777 (Census 2011). In 2014, 79.6% of KwaDela's residents made use of solid fuel burning for daily activities such as heating and cooking.

Instrumentation

A mobile monitoring station was used to obtain ambient concentrations of particulate matter (PM_{10} and $PM_{2.5}$ were measured using a MetOne BAM 1020, MetOne E-Bam and MetOne E-Samplers) and meteorological data (temperature, humidity, pressure, wind speed and direction, rainfall). The ambient monitoring site was located at the Secondary School close to the centre of KwaDela. Additionally two E-samplers were used to measure ambient PM concentrations ($PM_{2.5}$ and PM_{10}) in separate locations of the settlement.

The household considered in this study was semi-randomly chosen for indoor monitoring. Indoor particulate concentrations (PM_4) were measured using the TSI DustTrak (Models 8520 and 8530) photometric monitors, while the personal exposure of one of the residents in the household (PM_4) was monitored using the TSI SidePak AM510 photometric monitor. Temperature iButtons were placed in strategic locations within the sampling household to help better understand the indoor temperature dynamics. This included measuring temperatures in various rooms of the household (bedroom, kitchen, by the stove, and outside the house).

Sampling was conducted as part of a larger sampling campaign in KwaDela in various seasons (winter 2013 and 2014 and summer 2014 and 2015). This paper focuses on the measurements taken in one household in the winter 2014 campaign. This study was approved by the North-West University Research Ethics Committees (NWU-00066-13-S3).

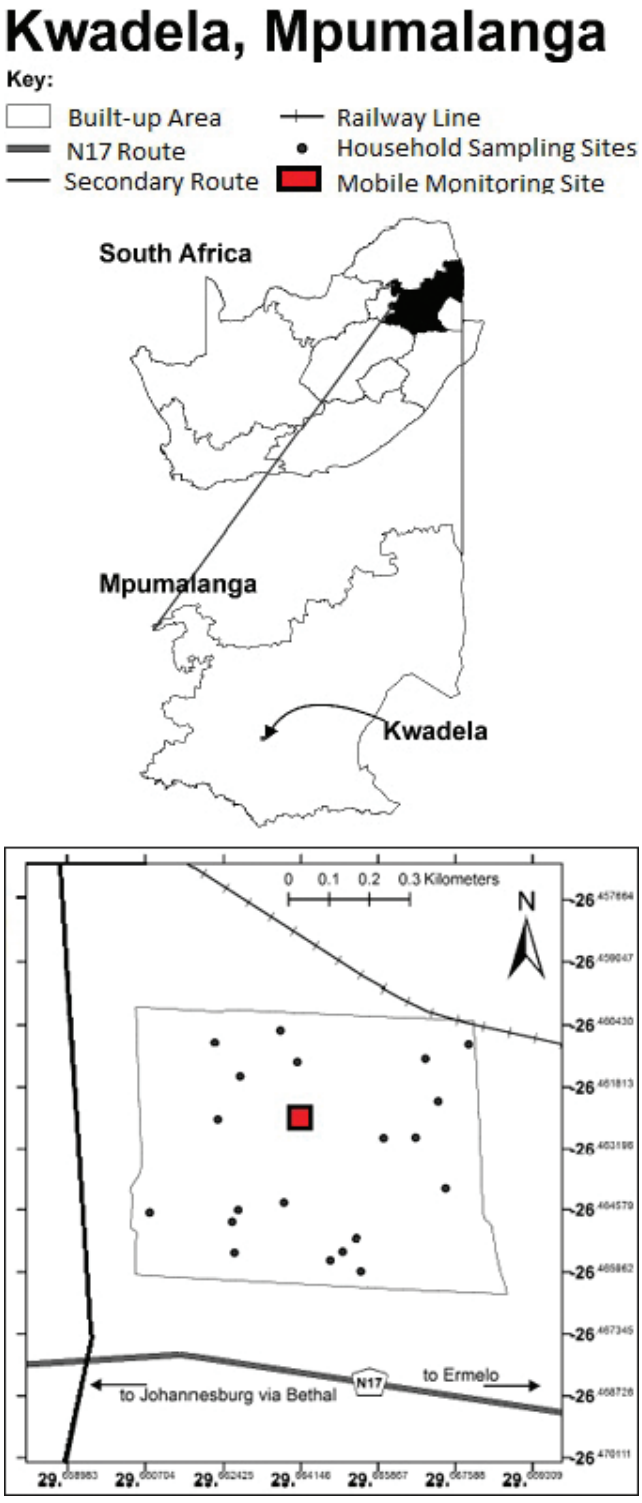

***Figure 1**: Map of Kwadela showing the distribution of household and mobile monitoring sites.*

Data Processing and Analysis

The data collected by the various instruments was merged into one overarching data set by synchronising the sampling intervals of the various instruments into an hourly data set. The instruments within the mobile monitoring station were checked once a week during the sampling. The indoor instruments were zero calibrated and flow checked as per manufacturer's

instructions. The personal monitoring instruments were flow checked once a week and zero calibrated each day before sampling.

Simple time series were plotted to identify the average diurnal PM patterns of the specific household. Furthermore, correlations between the indoor and outdoor and indoor and personal particulate concentration levels were found. Lastly, frequency distributions illustrated the 99th percentile of indoor and outdoor particulate concentrations.

The indoor and personal PM_4 measurements have been corrected according to the specific photometric calibration factors obtained for the DustTrak and SidePak instruments. It is noted that, as a possible limitation of this study, PM_4 and $PM_{2.5}$ are included as smaller fractions/ subsets of PM_{10}.

Results and Discussion

Exposure of residents to particulate matter

Mean outdoor $PM_{2.5}$ and PM_{10}, indoor PM_4 and personal PM_4 concentrations were 27±18 and 21±122 and 17±23 and 16±7 µg/m^3 respectively (Table 1). The variability of the particulate matter was highest for outdoor PM concentrations. 99th percentile values for outdoor $PM_{2.5}$, outdoor PM_{10}, indoor PM_4 and personal PM_4 concentrations were 81, 303, 126 and 30 µg/m^3 respectively. Frequency distributions indicate that the majority of all PM concentrations measured fall between 0 and 50 µg/m^3 (Figures 2-5).

***Table 1**: Descriptive Statistics of Outdoor, Indoor and Personal PM Measurements in (ug/m^3).*

	N	M	SD	Min	Max
O PM_{10} (ug/m^3)	178	48	122	1	1518
O $PM_{2.5}$ (ug/m^3)	274	27	18	2	196
I PM_4 (ug/m^3)	291	17	23	1	154
P PM_4 (ug/m^3)	7	16	7	10	112
N - Sample size M – Mean SD – Standard deviation Min – Minimum value Max – Maximum value O – Outdoor I – Indoor - P – Personal					

Relationship between indoor, outdoor and personal PM concentrations

The value of R^2 in the regression analyses in Figures 6 and 7 indicate a weak correlation between indoor and outdoor $PM_{2.5}$ concentrations (R^2 =0.087) and between indoor and outdoor PM_{10} concentrations (R^2=0.11). However, the correlation between personal and indoor PM is stronger at R^2=0.93 (Figure 8). This result limited by the fact that merely 7 measurements were available for this particular case. Regression analyses between the personal PM_4 and outdoor (PM_{10} and $PM_{2.5}$) measurements are not displayed here as there are too few data points for personal PM_4 to be representative of the true relationship.

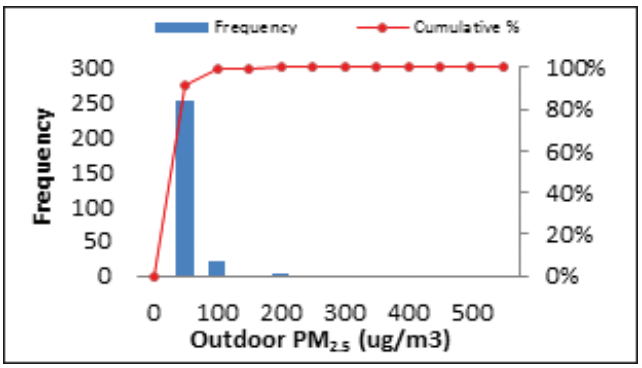

***Figure 2**: Distribution of mean 1-hourly outdoor $PM_{2.5}$ mass concentrations in µg/m^3.*

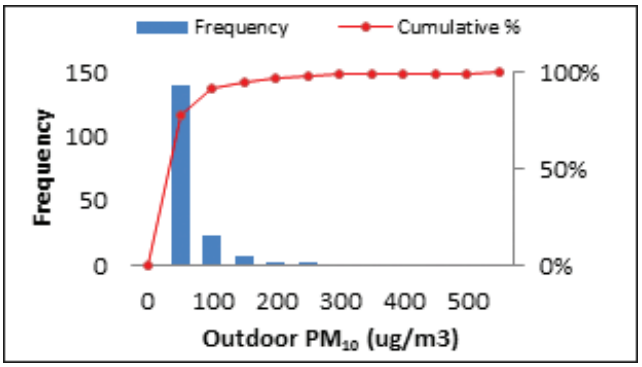

***Figure 3**: Distribution of mean 1-hourly outdoor PM_{10} mass concentrations in µg/m^3.*

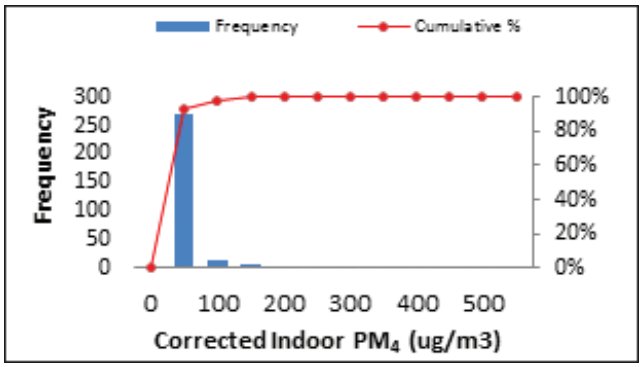

***Figure 4**: Distribution of mean 1-hourly indoor PM_4 mass concentrations in µg/m^3.*

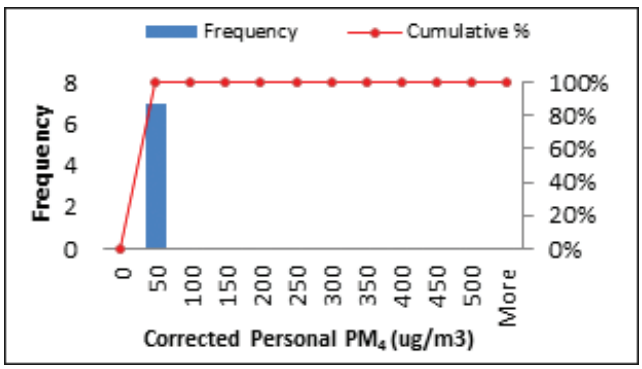

***Figure 5**: Distribution of mean 1-hourly personal PM_4 mass concentrations in µg/m^3.*

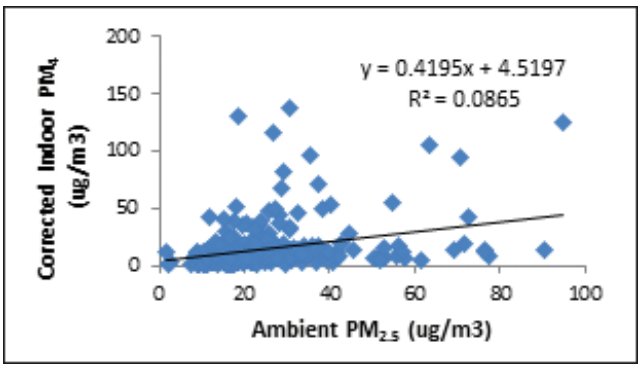

***Figure 6**: Regression analysis of indoor (PM_4) and outdoor ($PM_{2.5}$) concentrations in µg/m³.*

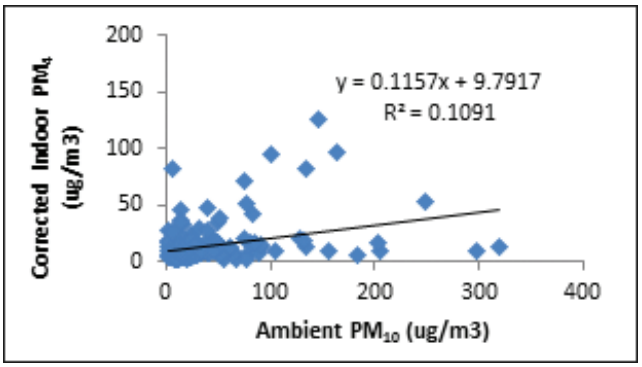

***Figure 7**: Regression analysis of indoor (PM_4) and outdoor (PM_{10}) concentrations in µg/m³.*

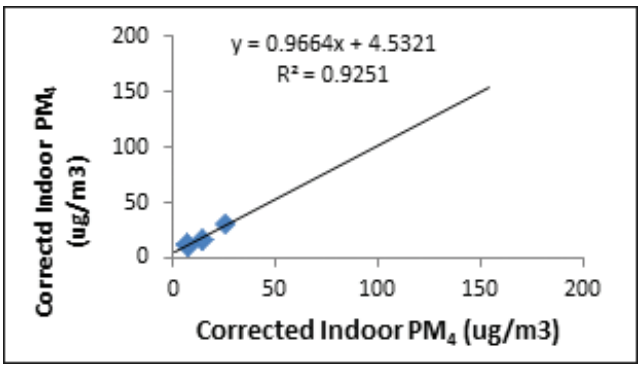

***Figure 8**: Regression analysis of personal and indoor PM_4 concentrations in µg/m³.*

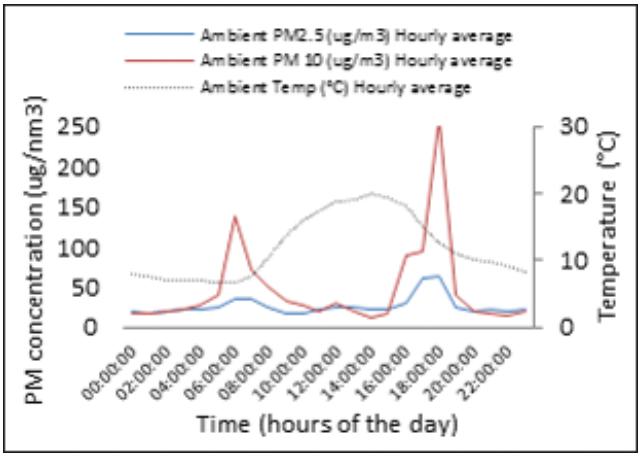

***Figure 9**: Hourly concentrations of outdoor particulate matter averaged during the winter period 7-19 August 2014.*

Diurnal patterns of exposure

Lower ambient temperatures and morning and evening time periods correspond with outdoor PM peaks (Figure 9). Higher stove temperatures link to cooking and heating activities in the early morning and afternoon hours as well as the evening hours with elevated indoor PM concentrations (Figure 10). Morning and evening peaks are also likely to be caused by vehicle emissions.

Indoor and outdoor PM concentrations follow a similar diurnal trend throughout the day, however, the mean PM_{10} hourly average concentrations lie above the mean outdoor $PM_{2.5}$ and indoor PM_4 concentrations. The visible diurnal trend is a signature trend for low level burning practices, indicating that all measured PM levels are directly influenced by solid fuel burning in the household and most likely by surrounding households. The differences in outdoor $PM_{2.5}$ and outdoor PM_{10} concentrations can most likely be attributed to the fact that the two monitoring instruments were located in different areas of KwaDela, being exposed to different ambient PM concentrations entirely.

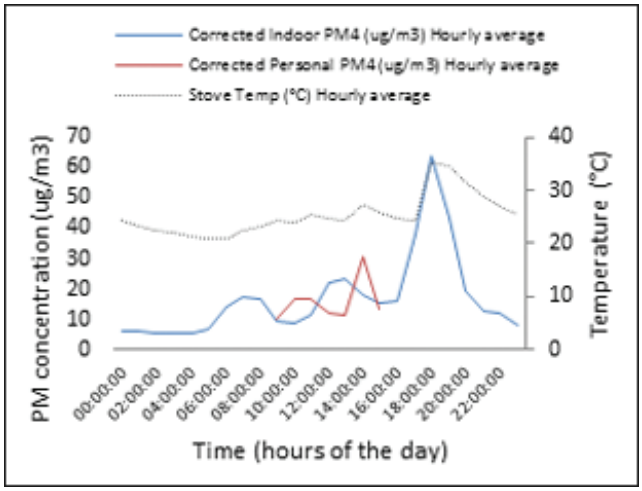

***Figure 10**: Hourly concentrations of indoor PM_4 averaged during the winter period 7-19 August 2014.*

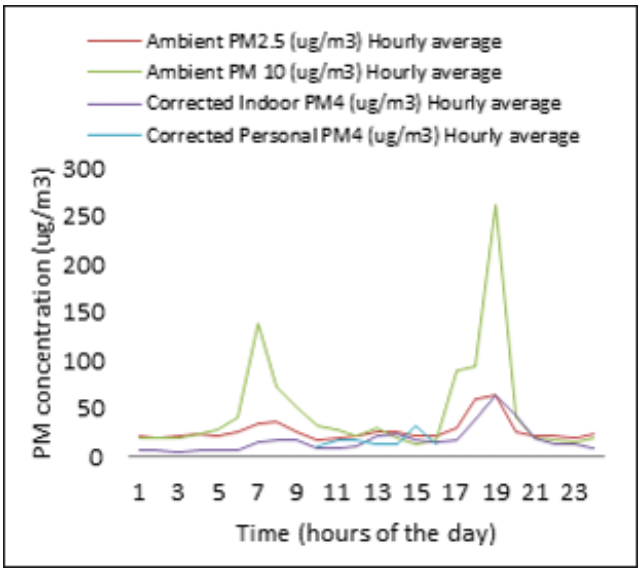

***Figure 11**: Hourly concentrations of indoor and outdoor PM concentrations averaged during the winter period 7-19 August 2014.*

Indoor and personal daily average PM_4 concentrations did not exceed the 24h National Ambient $PM_{2.5}$ Standard of 65 µg/m³ nor did they exceed the 24h National Ambient PM_{10} Standard of 75 µg/m³. The outdoor $PM_{2.5}$ concentrations were found to be below the standards for the duration of the sampling period. The outdoor PM_{10} concentrations exceeded the standards for one day during the sampling period (Figure 12).

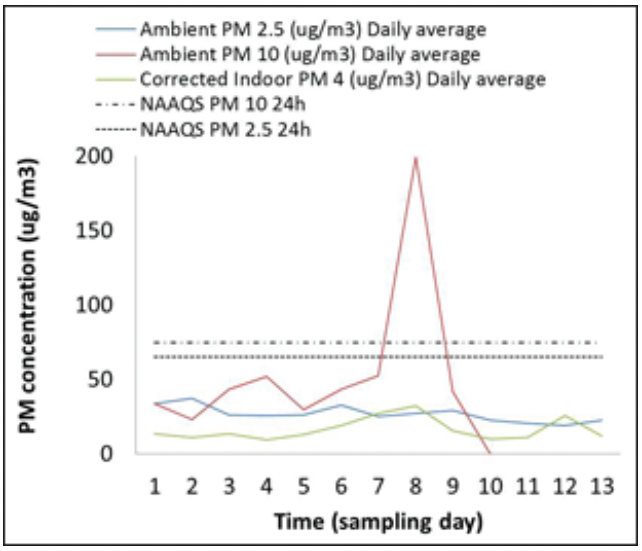

***Figure 12**: Daily average for PM concentrations measured against the NAAQS for PM_{10} and $PM_{2.5}$ over the sampling period.*

Conclusion

This study indicates that, in this household and during this sampling campaign, PM concentrations experienced outdoors were on average higher than those experienced indoors. Outdoor mean concentrations were 48 µg/m³ and 27 µg/m³ for PM_{10} and $PM_{2.5}$ and indoor mean concentrations were 17 µg/m³ and 16 µg/m³ for indoor and personal measurements respectively. Extreme events were evident in outdoor PM_{10} measurements where a maximum hourly value of 1518 µg/m³ was measured. Maximum hourly values for outdoor $PM_{2.5}$, indoor PM_4 and personal PM_4 were found to be 196 µg/m³, 15µg/m³ and 122 µg/m³ respectively.

Even though this study outlines the PM concentrations experienced at only one household, it gives an indication of the average indoor PM_4 concentrations an average person experiences in the Highveld, Mpumalanga, where the combustion of solid fuels is a daily practice occurring in the majority of households. This study indicates that people living in KwaDela are exposed to high PM concentrations which may exceed ambient PM standards outdoors, but that they are exposed to high PM concentrations even indoors, which may be detrimental to their health.

Acknowledgments

The data collection was conducted by Richhein Du Preez, Corné Grové and Brigitte Language from North West University and The NOVA Institute under the supervision of Professor Stuart Piketh for Sasol's air quality offset pilot study.

References

Bruce, N., Pope, D., Rehfuess, E., Balakrishnan, K., Adair-Rohani, H. and Dora, C. 2015, 'WHO indoor air quality guidelines on household fuel combustion: strategy implications of new evidence on interventions and exposure – risk functions', *Atmospheric Environment* 106: 451-457.

Diapouli, E., Eleftheriadis, K., Karanasiou, A., Vratolis, S., Hermansen, O., Colbeck, I. and Lazaridis, M. 2011, 'Indoor and Outdoor Particle Number and Mass Concentrations in Athens. Sources, Sinks and Variability of Aerosol Parameters', *Aerosol and Air Quality Research* 11:632–642.

Chafe, Z.A., Brauer, M., Klimont, Z., Van Dingenen, R., Mehta, S., Rao, S., Riahi, K., Dentener, F. and Smith, K.R., 2014, 'Household Cooking with Solid Fuels Contributes to Ambient $PM_{2.5}$ Air Pollution and the Burden of Disease', *Environmental Health Perspectives* 122:1314-1320.

Ferro, A.R., Kopperud, R.J., Hildemann, l.M. 2004, 'Elevated personal exposure to particulate matter from human activities in a residence', *Journal of Exposure Analysis and Environmental Epidemiology* 14:34–40.

Lim S.S, Vos T, Flaxman AD, Danaei G, Shibuya K, Adair-Rohani H, et al. 2012, 'A comparative risk assessment of burden of disease and injury attributable to 67 risk factors and risk factor clusters in 21 regions, 1990–2010: a systematic analysis for the Global Burden of Disease Study 2010', *The Lancet* 380:2224-60.

Medical Research Council, 2008, 'South Africa Comparative Risk Assessment' *Summary Report*.

Norman R, Barnes B, Mathee A, Bradshaw D and the South African Comparative Risk Assessment Collaborating Group. 2000, 'Estimating the burden of disease attributable to indoor air pollution in South Africa in 2000', *South African Medical Journal*, 97:764-771.

Smith, K.R. 2000, 'National burden of disease in India from indoor air pollution', *PNAS* 24:13286–13293.

Smith, K.R.2002, 'Indoor air pollution in developing countries: Recommendations for research', *Indoor Air* 12:198-207.

Terblanche, A.P.S., Nel, R., Reinach, G., and Opperman, L. 1992, 'Personal exposures to total suspended particulates from domestic coal burning in South Africa', *The Clean Air Journal* 8(6):15-17.

Xie, Y., Zhao, B., Zhang L. and Luo, R. 2015, 'Spatiotemporal variations of $PM_{2.5}$ and PM_{10} concentrations between 31 Chinese cities and their relationships with SO_2, NO_2, CO and O_3', *Particuology* 20:141–149.

Climate change impacts on mean wind speeds in South Africa

Lynette Herbst[*1,2] **and Hannes Rautenbach**[2]
[1] Department of Engineering and Technology Management, University of Pretoria,
Cnr Lynnwood Rd and Roper Str, Hatfield, Pretoria, 0001, South Africa, lynette.herbst@up.ac.za
[2]Laboratory for Atmospheric Sciences, Department of Geography, Geoinformatics and Meteorology,
University of Pretoria, hannes.rautenbach@up.ac.za

Received: 16 October 2015 - **Reviewed:** 19 November 2015 - **Accepted:** 24 November 2015
http://dx.doi.org/10.17159/2410-972X/2015/v25n2a2

Abstract
Climate change could potentially affect a number of variables that impact the dispersal of and human exposure to air pollutants, as well as climate dependent sectors such as wind energy. This study attempted to quantify the projected changes in seasonal daily mean wind speeds for South Africa around the mid-21st century (2051-2075) under two different atmospheric heat pathways. Seasonal daily mean wind speed increases rarely reach 6% and decreases occur to a maximum of 3% and are variable between different seasons and areas within the country. In all seasons except December-January-February, wind speeds are projected to increase in the Highveld region, suggesting that air pollution dispersing conditions could increase. Wind direction at the 850hPa-level show minor changes, except over the Western and Eastern Cape provinces.

Keywords
climate change, wind speed, air pollution, mitigation, climate models

Introduction
Changes in climate could affect local and regional air pollution concentrations by impacting atmospheric chemical reactions, transport and rates of dispersion of *inter alia* acidic materials (Bernard et al., 2001). The South African government aims to cut greenhouse gas (GHG) emissions by 42% by 2025 by implementing a range of climate change mitigation strategies, including renewable energy of which wind and solar resources are highly dependent on climate. If the country achieves this goal and successfully executes its plan to contribute 30% renewable energy to the country's energy mix by 2025, it would contribute substantially to reducing air pollution. Horton et al. (2014) suggest that large parts of South Africa could expect pollutant-dispersing conditions more often as the 21st century progresses, but their work had been conducted with global climate models (GCMs) on an annual scale.

However, variations in wind climates could occur within finer spatial scales than are represented by GCMs, and finer temporal scales than are represented by assessments at annual intervals. Therefore, the work presented in this study employed an ensemble of eight GCMs that have been dynamically downscaled to regional climate model (RCM) resolution (0.44° × 0.44°).

This study had two objectives. Firstly, to evaluate the representation of past climates by state-of-the-art climate models at a regional scale by verifying them against observational data during a 25-year reference period (1981-2005). Secondly, to establish whether notable changes exist between seasonal wind speeds at surface level and wind direction at the 850hPa-level during the reference period and a future period (2051-2075) under two atmospheric heat pathways, RCP4.5 and RCP8.5.

Data and Methods

Data
In order to address the research objectives, two CO_2 RCP pathways were considered in eight dynamically downscaled GCM simulations from the Intergovernmental Panel on Climate Change (IPCC) fifth assessment report (AR5) to determine the potential influence of global warming on South African winds. The Rossby Centre, a climate modelling research unit at the Swedish Meteorological and Hydrological Institute, has produced a substantial collection of regional climate model simulations for the African region through dynamical downscaling of a subset of eight GCMs from the CMIP5 initiative. These downscaled model simulations were produced by the Rossby Centre's RCA4 RCM.

The initiative formed part of the CORDEX-Africa (COordinated Regional Downscaling EXperiment) project. The forcing GCMs were the CanESM2, CNRM-CM5, EC-EARTH, MIROC5, HadGEM2-ES, MPI-ESM-LR, NorESM1-M, and GFDL-ESM2M coupled GCMs. Winds simulated by models are susceptible to large errors, hence the use of eight models: a multi-model ensemble allows a

more robust assessment (Rasmussen et al., 2012, Pašičko et al., 2012). RCA4 RCM data are available for a historical period from 1951 to 2005, and a projected period from 2006 to 2100.

The implementation of climate change mitigation measures could also affect the manner in which wind climates behave. Fant et al. (2015) emphasise that the probability of small wind speed changes increases considerably under a climate change scenario that incorporates mitigation strategies. Therefore, the model output of this project was considered in terms of two atmospheric heat pathways (RCP4.5 and RCP8.5). In the AR5, GHG emissions pathways considered were expressed in terms of these atmospheric heat based Representative Concentration Pathways (RCPs). IPCC scenarios (SRES) used in previous assessment reports (based on CO_2 concentrations) could be updated in the AR5 to heat based pathways thanks to new information on emerging technology, economies, land use, land cover change and environmental factors of almost a decade (Moss et al., 2010). The new AR5 GHG forcing for future projections used in this study consist of CO_2 RCPs related to 4.5W.m^{-2} and 8.5W.m^{-2} atmospheric heat increases by 2100 (henceforth RCP4.5 and RCP8.5, respectively), amongst other pathways. The use of the word 'representative' resembles the fact that each RCP signifies one of numerous possible scenarios leading to particular radiative forcing characteristics (Van Vuuren et al., 2011). The word 'pathway' refers to the trajectory taken over a long time to achieve a given radiative forcing point in terms of long-term GHG concentration levels. Such time-evolving concentrations of radiatively active constituent pathways could be incorporated for driving global warming climate model simulations.

In more detail, RCP4.5 (and RCP8.5) represents a radiative forcing of ~4.5W.m^{-2} at stabilisation after 2100 (>8.5W.m^{-2} in 2100) and a ~650ppm CO_2-equivalent concentration at stabilisation after 2100 (>1370ppm CO_2-equivalent in 2100). RCP4.5 therefore represents a pathway that stabilises without overshoot, and RCP8.5 resembles a rising pathway. RCP4.5 was developed by the Global Change Assessment Model (GCAM) of the Pacific Northwest National Laboratory in the USA, while the RCP8.5 was developed by the Model for Energy Supply Strategy Alternatives and their General Environmental impact (MESSAGE) from the International Institute for Applied Systems Analysis in Austria (Moss et al., 2010). These RCPs are two of four which were used in AR5.

In order to identify model biases, RCA4 RCM output had to be assessed through comparison with observational data such as the ECMWF (European Centre for Medium-range Weather Forecasts) ERA-Interim global reanalysis data, which is a global atmospheric reanalysis available from 1979 to present. Its grid resolution is 0.75° × 0.75°. To examine changes in, for example, mean daily wind speeds, 30-year assessment periods are preferred to comply with the World Meteorological Organisation's definition for 'climate'. Since ERA-Interim reanalysis data is available from 1979 onwards, and the historical period for the RCA4 model output ends in 2005, a 25-year assessment period (1981-2005) was chosen for this study, which was then compared to a projection period (2051-2075).
ERA-Interim reanalysis data are particularly useful in climate change assessments as it covers numerous climate variables in a coherent structure. Observational data used in the reanalysis originate from inter alia wind profilers, pilot balloons, radiosondes, land stations, aircraft, ships and drifting buoys (Dee et al., 2011).

Methods

ERA-Interim reanalysis data

Model performance was evaluated by calculating differences between the RCA4 output and ERA-Interim reanalysis data. For this purpose, daily (00:00UCT, 06:00UCT, 12:00UCT and 18:00UCT) historical near-surface (10m above ground level (agl)) u- and v-components have been obtained for the 25-year period 1981 to 2005, across the domain 18° to 42°S and 14° to 37°E, from the ERA-Interim reanalysis databank. For comparing RCA4 RCM output (0.44° × 0.44° resolution) to ERA-Interim reanalysis data (0.75° × 0.75° resolution), ERA-Interim reanalysis fields were interpolated (bilinear) to fit the RCA4 fields. The ERA-Interim simulation domain size was also modified to correspond with the RCA4 domain. The boundaries of this domain are 19.5° to 40.5°S and 15° to 35.25°E.

Wind speed (ws) was calculated from u- and v-components as follows:

$$ws = \sqrt{u^2 + v^2} \quad (1)$$

Wind speeds at 00:00UCT, 06:00UCT, 12:00UCT and 18:00UCT were averaged to obtain daily means, which were compatible with RCA4 RCM data: RCA4 data is provided as daily averages taken eight times a day, i.e. three-hourly (Christensen et al., 2014). The first 28 days of each month were then selected for further calculation. Residual days could not be used in the analysis, due to the fact that some model fields consist of 30-day months only, while others included leap years. A uniform month-day number was important for calculating cross-model ensemble averages. Seasonal wind speeds were then obtained after categorising daily data into four groups: December-January-February (DJF), March-April-May (MAM), June-July-August (JJA) and September-October-November (SON). From this, seasonal daily mean wind speeds for each season were calculated.

Model data

Data from eight the GCMs that were dynamically downscaled using the RCA4 RCM were obtained. A domain extending from 22° to 35°S and 16.2° and 33°E was defined for the study. Daily historical near-surface wind speeds (10m agl) were extracted for each model for the 25 years extending from 1981 to 2005. For each of these eight model files, data were grouped into seasons (DJF, MAM, JJA and SON). Days 1 to 28 were then extracted, as explained previously, for each month per season and per model.

Thereafter, ensemble means of the daily data were calculated from the eight RCA4 RCM simulations across the four seasons, from where daily mean wind speeds for each of the seasons were calculated.

To project potential diversions from dominant wind directions, the u- and v-components at the 850hPa-level were extracted for each model for the 25 years extending from 1981 to 2005 as well. The data were grouped seasonally, extracted from days 1 to 28, and ensemble means were calculated according to the same procedure followed for the near-surface wind speed data. The u- and v-component data were then used as vectors in the Grid Analysis and Display System (GrADS) to calculate and display wind directions for the historical period of 1981 to 2005.

Statistical evaluation of model performance

In order to verify RCA4 RCM performance, the Root Mean Square Error (RMSE) of seasonal daily mean wind speeds were calculated using the ERA-Interim and the RCA4 RCM data. RMSE was calculated as follows (CTEC, 2015):

$$RMSE = \sqrt{\sum_{i=1}^{n} \frac{(x_{obs,i} - x_{model,i})^2}{n}} \quad (2)$$

where $x_{obs,i}$ represents the observed ERA-Interim values; $x_{model,i}$ represents the model values at a particular point i; and n represents the number of values.

Model evaluation against observational data

RCA4 RCM output was evaluated against observational data from six South African Weather Service (SAWS) stations distributed across the country. Data from Malmesbury, Vredendal, Greytown, Upington, Nelspruit, and Mokopane were obtained from SAWS for varying periods starting in 1981 to 2005. Wind speeds were estimated visually from pressure plate anemometers until 1992 (excluding Upington), when wind speeds began to be measured with Automatic Weather Stations (AWS), and are therefore more accurate. The data were provided as it was measured at 08:00, 14:00 and 20:00. These three times daily observations were averaged to obtain single daily averages, which were then employed in calculating seasonal average wind speeds. Model values for comparison were selected from those grid boxes in model data within which the particular weather station's coordinates lie. These coordinates are shown in Table 1, as well as the period for which data were available. Note that two stations' data were considered for the Upington area, as the periods of availability of both differ.

***Table 1**: SAWS weather station particulars*

Station name	Coordinates	Period of data availability
Malmesbury	33.4720 S 18.7180 E	1986/02-2005/12
Vredendal	31.6730 S 18.4960 E	1981/01-2005/12
Greytown	29.0830 S 30.6030 E	1993/03-2005/12
Upington (1) Upington (2)	WK 28.4000 S 21.2670 E WO 28.4110 S 21.2640 E	1981/01-1992/04 1991/07-2005/12
Nelspruit	25.5030 S 30.9110 E	1993/07-2005/12
Mokopane	24.2050 S 29.0110 E	1995/09-2005/12

Changes in wind climate

Daily means of seasonal near-surface wind speed, in the projected period were calculated from RCA4 RCM output under conditions of the RCP4.5 and RCP8.5 pathways. Data for 850hPa-level u- and v-components were obtained for these pathways as well. The data were extracted and grouped in the same manner as in the historical period, but in this case for a 25-year period extending from 2051 to 2075.

Anomalies between RCA4 RCM output in the reference period and RCA4 RCM output in the two projections were calculated and expressed as percentage differences. Wind direction changes at the 850hPa-level were also calculated for the two RCPs by subtracting historical u/v components from projected u/v components, and then by using these anomalies to plot deviations from the dominant wind direction in the reference period.

Results

Mean seasonal wind speed

For the DJF-season, the winds in the north-western quarter of the country are captured well, showing wind speeds in the region of 4m.s^{-1} to 5m.s^{-1} in both ERA-Interim (Figure 1) and RCA4 RCM ensemble (Figure 2) runs. However, wind speeds are somewhat overestimated over the eastern escarpment by the RCA4 RCM. The ERA-Interim simulation shows that near-surface winds occur at around 1.5m.s^{-1} to 3.5m.s^{-1}, whereas the RCA4 RCM simulations project winds in this area to vary from 3m.s^{-1} to 5m.s^{-1}. Furthermore winds are projected at around 3m.s^{-1} to 5m.s^{-1} in the ERA-Interim run, but the RCA4 RCM projection ranges from 4.5m.s^{-1} to 6m.s^{-1} in the south-east of the country by the model data. In summary, the RCA4 RCM projects near-surface wind speeds at around 1.5m.s^{-1} higher than observed data shows it to be, except in the north-western quarter of the country.

In the MAM-season, the lower wind speeds occurring from central South Africa to the Highveld are well captured by the RCA4 RCM, with only a 1m.s^{-1} difference between ERA-Interim (Figure 3) and RCA4 RCM (Figure 4) output, the latter projecting the higher mean wind speed. An overestimation of wind speeds by the RCA4 RCM is observed along a west-east strip stretching from the Cape Town region to Lesotho. According to the ERA-Interim simulation, wind speeds range from 2.5m.s^{-1} to 4m.s^{-1}, and the RCA4 RCM projects wind speeds to range from 3.5m.s^{-1} to 5.5m.s^{-1}. Wind speed projection ranges therefore are estimated by the RCA4 RCM by no more than 1.5m.s^{-1} higher than ERA-Interim data in this season.

Near-surface wind speeds in the JJA-season are projected at no less than 2.5m.s^{-1} in the north-eastern quarter of the country in the RCA4 RCM ensemble run (Figure 6) – 0.5m.s^{-1} higher than the ERA-Interim run (Figure 5). The west-east strip RCA4 RCM ensemble overestimation observed from Cape Town to Lesotho in the MAM-season (Figure 4) is also present in the JJA-season:

the ERA-Interim run shows that these winds range from 3m.s^{-1} to 5m.s^{-1}, while the RCA4 RCM ensemble run shows it could range from 3.5m.s^{-1} to 6m.s^{-1}.

Finally, in the SON-season lower wind speeds in the south-eastern tip of the country are once more not well captured by the RCA4 RCM, nor is it represented along the eastern escarpment stretch (Figure 8). The simulation from the ERA-Interim data (Figure 7) suggests that winds range from 2m.s^{-1} to 5m.s^{-1}, but they range from 3.5m.s^{-1} to 6m.s^{-1} in RCA4 RCM ensemble run. On the other hand, winds over the central part of the country are well captured, as they occur at about 3.5m.s^{-1} to 4.5m.s^{-1} in both ERA-Interim and model ensemble runs.

The RMSE of seasonal mean daily near-surface wind speeds (m.s^{-1}) are shown in Figures 9 to 12. The high RMSE values on the south-eastern tip of the country demonstrate overestimations identified in previous paragraphs in all seasons. In general, it is confirmed that the RCA4 RCM performs best over central South Africa. The MAM-season has the largest area with the lowest RMSE, mostly between 0.8m.s^{-1} and 1.6m.s^{-1} (Figure 10). The highest RMSE-values of 2.8m.s^{-1} occur in the JJA-season in the Cape Town region and Lesotho (Figure 11).

Model evaluation against observational data

Mean daily wind speeds as simulated from RCA4 RCM data, plotted together with mean daily wind speeds calculated from ground station data recorded at six SAWS weather stations are shown in Figure 13. Four separate values were plotted per location according to seasons. Wind speeds from RCA4 RCM ensemble data at all of the points plotted were higher than the observational data from the SAWS weather stations. It must be borne in mind that wind speeds vary markedly on scales smaller than the grid resolution of model data of 0.44º × 0.44º (0.44º latitude translates roughly to between 45 and 40km; 0.44º longitude to 49km). Minor topographical variations, land cover and temperature variations can intensify or slow winds (Jarvis and Stuart, 2001). The model performs best at the Upington region and Mokopane regions (locations 13-16 and 21-24, respectively in Figure 13). The overestimation of winds demonstrated by the high RMSE-values in previous figures in the Western Cape region (Figures 9 to 12) are supported by the large differences in Malmesbury and Vredendal observations versus model output in Figure 13 (locations 1-4 and 5-8, respectively).

RCA4 RCM projected mean seasonal wind speed and direction changes

For the DJF-season, it is shown in Figure 14 that wind speeds are expected to increase by up to 4% along the southern parts of the Western and Eastern Cape Provinces under RCP4.5 (Figure 14). For the RCP8.5 pathway, increases in wind speeds could reach 6% in this area (Figure 15). Decreases in wind speeds of up to 1.5% might be expected in the Highveld under the RCP4.5 pathway (Figure 14) and 2.5% under the RCP8.5 pathway (Figure 15).

In the MAM-season under the RCP4.5 pathway, wind speeds are projected to increase by up to 3.5% in the north-eastern quarter of the country, and could also increase by up to 3% in the Cape Town region (Figure 16). Projected increases in wind speeds are more apparent in the RCP8.5 pathway in these regions, where it could increase by up 5% in the Limpopo province and 4.5% in the Cape Town region (Figure 17). The central part of the country could expect a slight increase in wind speeds of about 1% to 3% under the RCP8.5 pathway as well (Figure 17). Decreased wind speeds are projected under the RCP4.5 pathway in the Northern Cape and the Eastern Cape Provinces, but of only 1% (Figure 16). In the RCP8.5 pathway it is projected that the western half of the Northern Cape Province could expect decreased wind speeds of up to 2% and the Eastern Cape Province could expect wind speeds to increase by 2% along the coast, and decrease by 1% closer to the escarpment edge over the east of South Africa (Figure 17).

In the RCP4.5 pathway in the JJA-season, wind speeds are projected to increase for the majority of the country (Figure 18). Specifically the eastern half of the country could expect wind speeds to increase by up to 4.5%, but central South Africa and the Cape Town region could expect wind speeds to increase by up to 3%. Decreased wind speeds of up to 1% are projected in this same pathway over the coastal Eastern Cape Province and the West Coast. Under the RCP8.5 pathway, wind speeds are projected to increase by up to 6% in the far east of South Africa, and in the region of 1% to 3% in the interior (Figure 19). Wind speeds are projected to decease along the West Coast by up to 2%, and could decrease by 1.5% in the Eastern Cape Province.

In the SON-season, wind speeds are projected to increase by 5% in the Limpopo Province, and lesser increases are projected along the South African coast starting at KwaZulu-Natal all the way to Cape Town under the RCP4.5 pathway (Figure 20). The region around and included the Northern Cape Province could expect wind speeds to increase by 0% up to 1.5%. Under the RCP8.5 pathway, the Limpopo Province could expect wind speeds to increase by up to 6% (Figure 21). The rest of the country could expect milder wind speed increase ranging from 0.5% in parts of the Northern Cape Province, to 4% in the Cape Town region and central South Africa. Thus wind speeds are not projected to decrease under either of the pathways for the SON-season.

In the DJF-season, the north-easterlies over the Gauteng region (Figure 2) are projected to deviate towards the east in the RCP4.5 (Figure 14) and the RCP8.5 (Figure 15) pathway. Over the western half of the country, the southerlies (Figure 2) are projected to deviate in an east to south-eastern direction in the interior of the country under both pathways (Figures 14 and 15). The southerlies close to the coast in the Western Cape (Figure2) are projected to deviate to the west in both pathways as well (Figures 14 and 15). The south-easterlies simulated in the far eastern corner of the country are projected to deviate to the east in the RCP4.5 pathway (Figure 14) and are projected to deviate in an easterly to north-easterly direction in the RCP8.5 pathway (Figure 15).

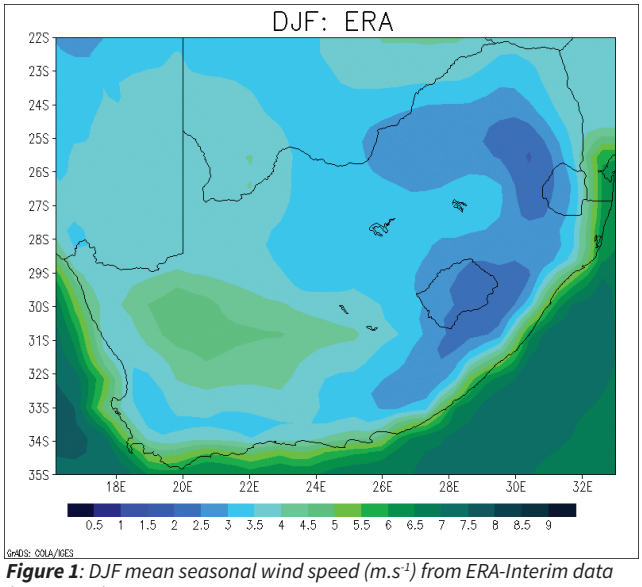

***Figure 1**: DJF mean seasonal wind speed (m.s^{-1}) from ERA-Interim data (1981-2005)*

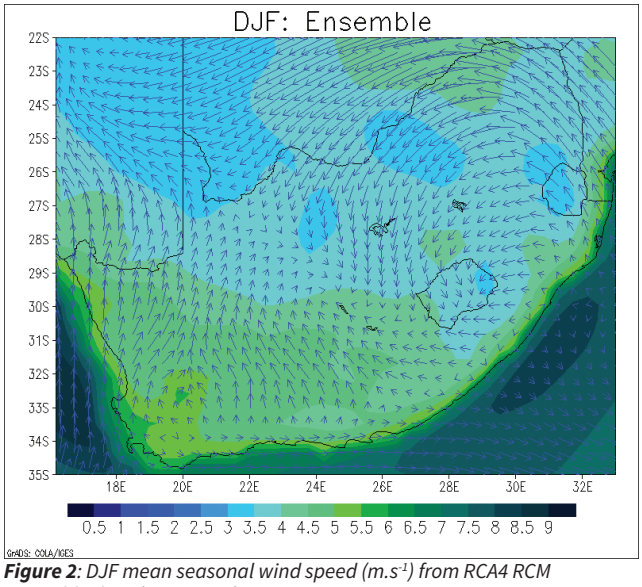

***Figure 2**: DJF mean seasonal wind speed (m.s^{-1}) from RCA4 RCM ensemble data (1981-2005).*

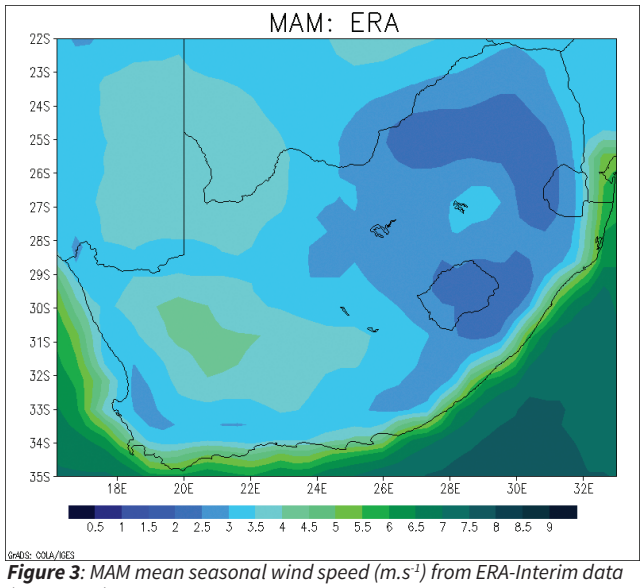

***Figure 3**: MAM mean seasonal wind speed (m.s^{-1}) from ERA-Interim data (1981-2005).*

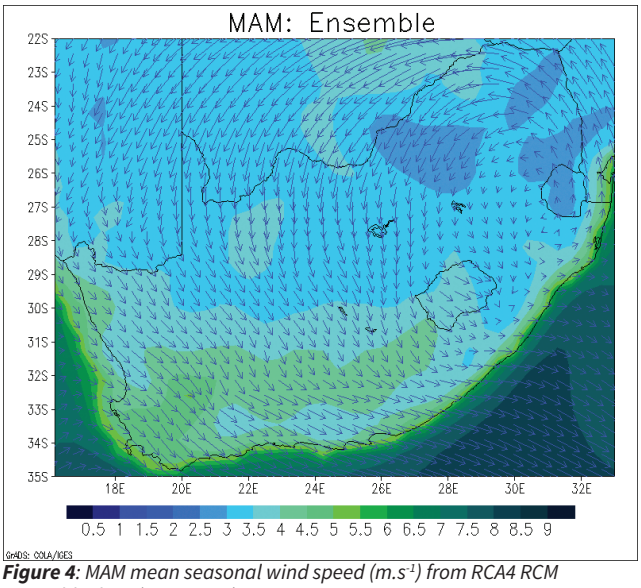

***Figure 4**: MAM mean seasonal wind speed (m.s^{-1}) from RCA4 RCM ensemble data (1981-2005).*

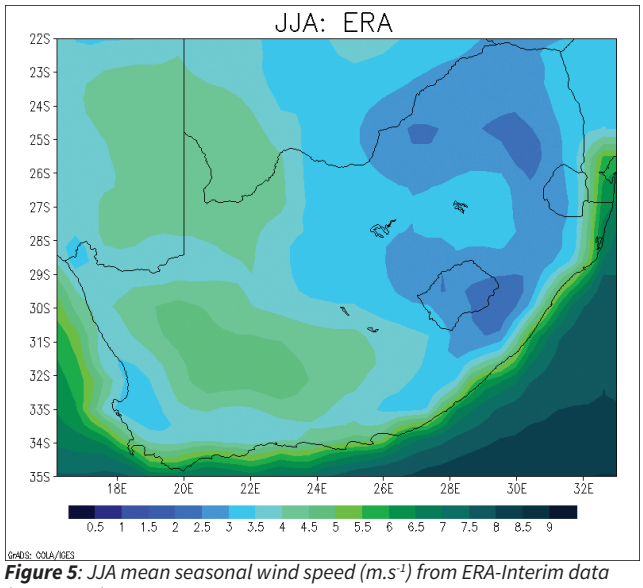

***Figure 5**: JJA mean seasonal wind speed (m.s^{-1}) from ERA-Interim data (1981-2005).*

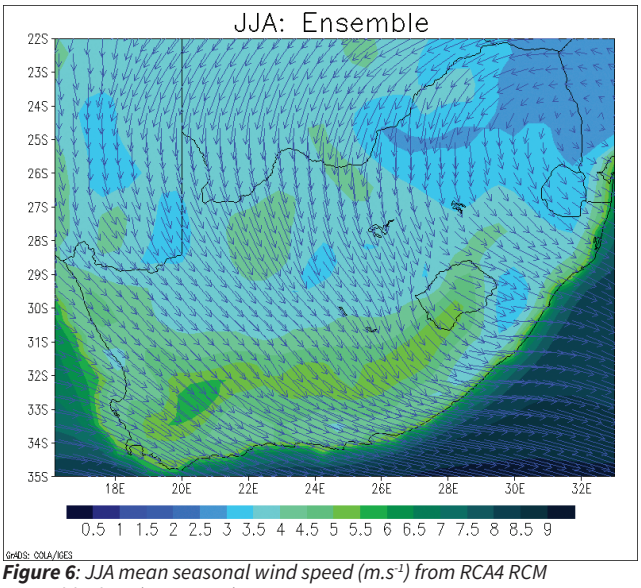

***Figure 6**: JJA mean seasonal wind speed (m.s^{-1}) from RCA4 RCM ensemble data (1981-2005).*

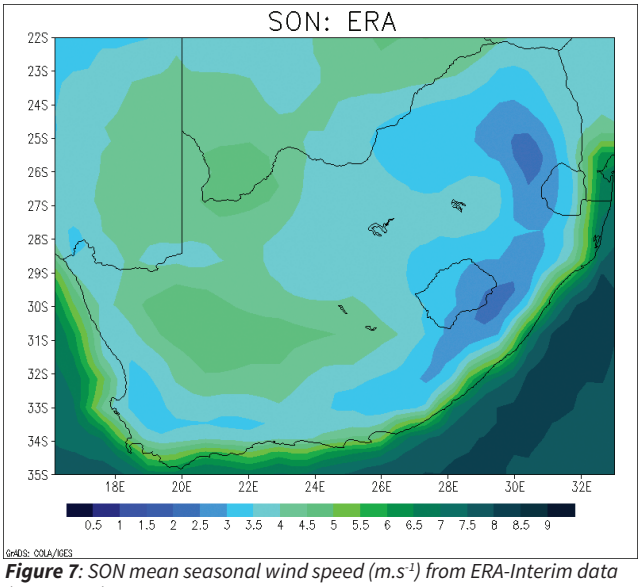

***Figure 7**: SON mean seasonal wind speed (m.s^{-1}) from ERA-Interim data (1981-2005).*

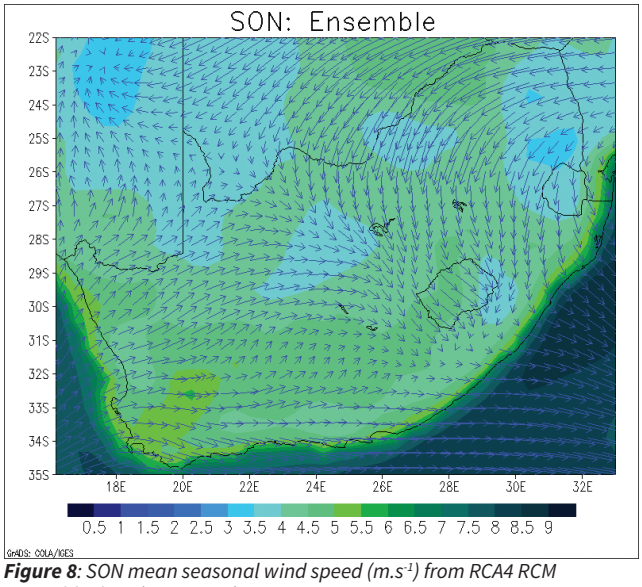

***Figure 8**: SON mean seasonal wind speed (m.s^{-1}) from RCA4 RCM ensemble data (1981-2005).*

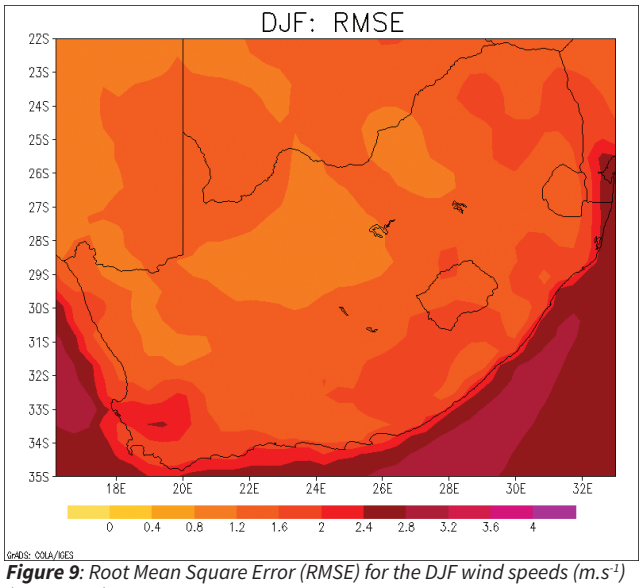

***Figure 9**: Root Mean Square Error (RMSE) for the DJF wind speeds (m.s^{-1}) (1981-2005).*

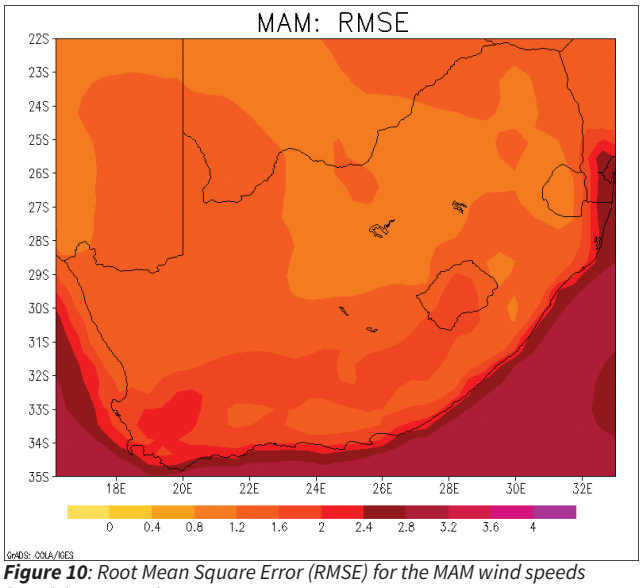

***Figure 10**: Root Mean Square Error (RMSE) for the MAM wind speeds (m.s^{-1}) (1981-2005).*

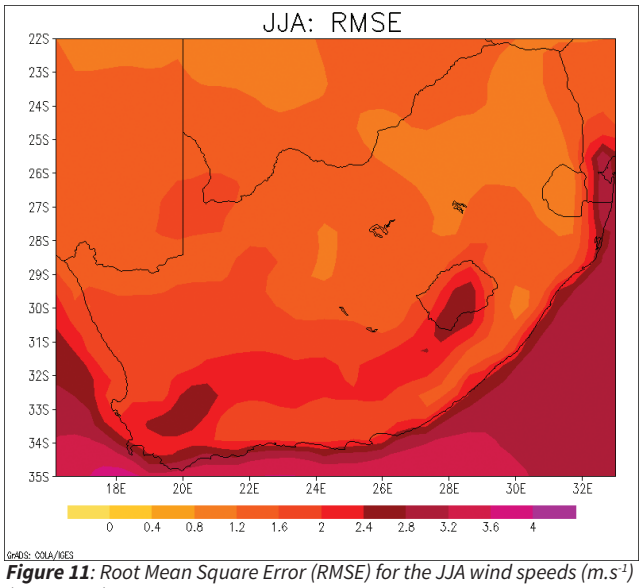

***Figure 11**: Root Mean Square Error (RMSE) for the JJA wind speeds (m.s^{-1}) (1981-2005).*

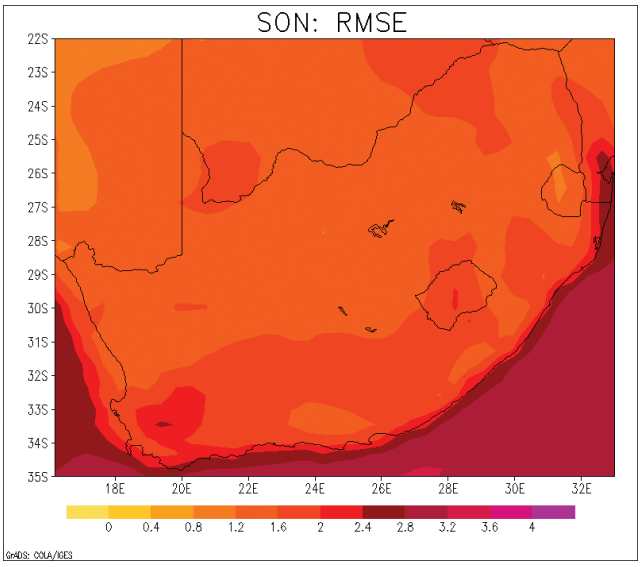

***Figure 12**: Root Mean Square Error (RMSE) for the SON wind speeds (m.s^{-1}) (1981-2005).*

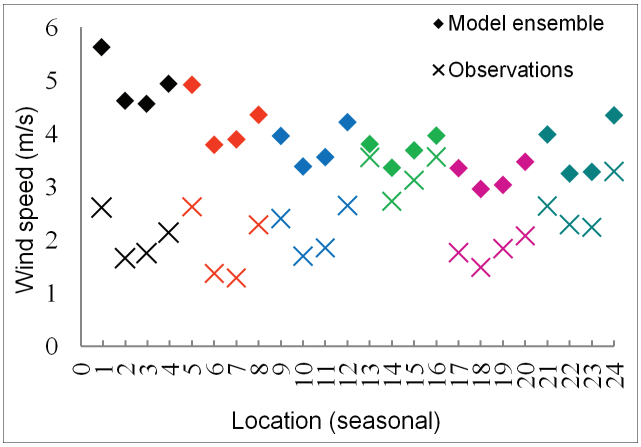

***Figure 13**: Comparison of wind speeds from SAWS station data with RCA4 RCM ensemble data. Location numbers 1-4 denote Malmesbury DJF, MAM, JJA, SON; location numbers 5-8 denote Vredendal DJF, MAM, JJA, SON etc. - in the same order as in Table 1.*

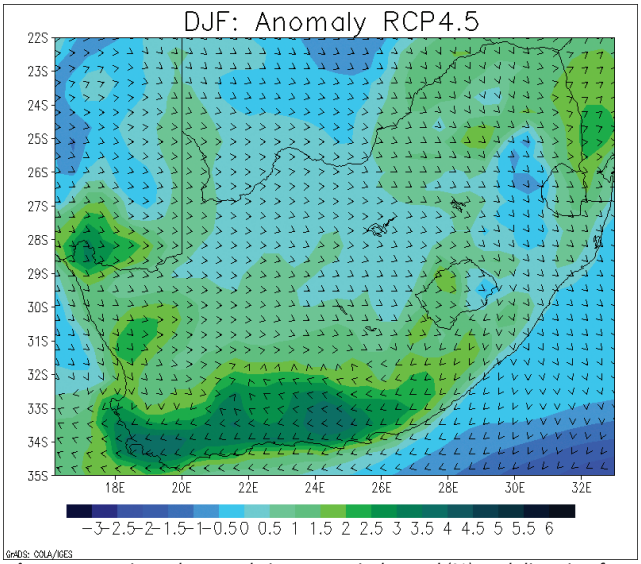

***Figure 14**: Projected anomaly in mean wind speed (%) and direction for DJF (2051-2075 relative to 1981-2005) under the RCP4.5 pathway.*

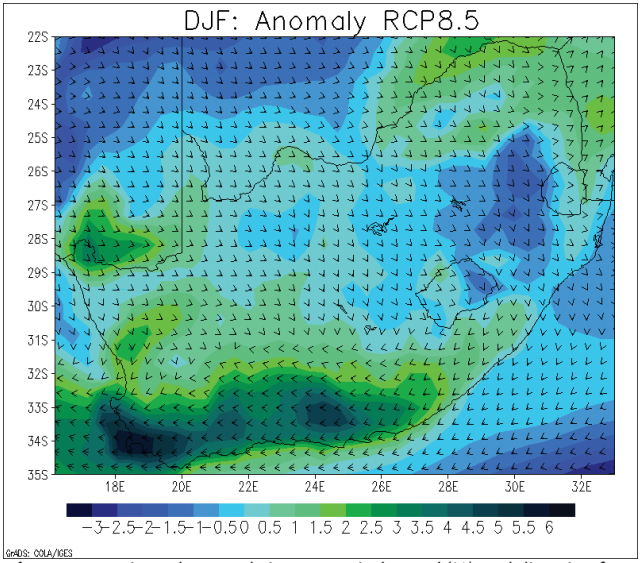

***Figure 15**: Projected anomaly in mean wind speed (%) and direction for DJF (2051-2075 relative to 1981-2008) under the RCP8.5 pathway.*

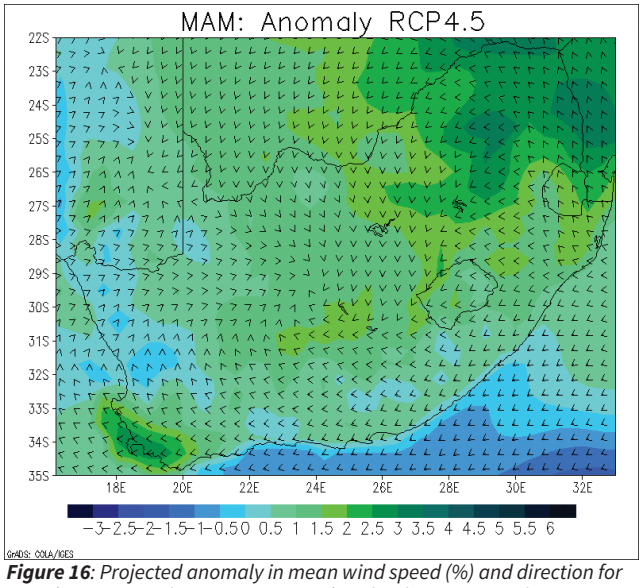

***Figure 16**: Projected anomaly in mean wind speed (%) and direction for MAM (2051-2075 relative to 1981-2005) under the RCP4.5 pathway.*

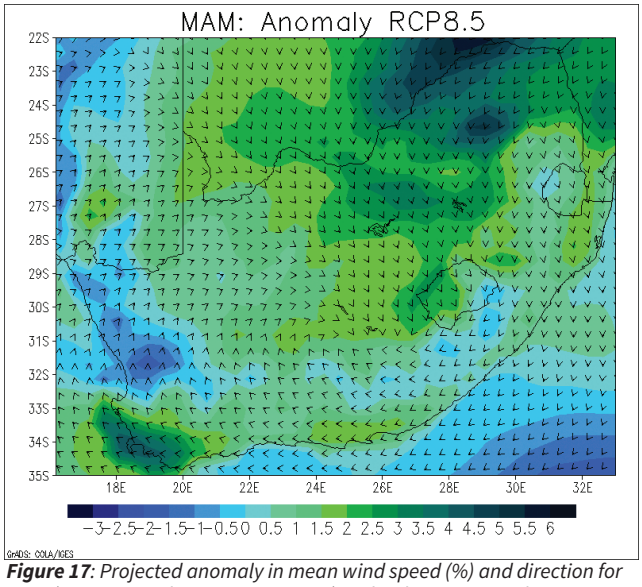

***Figure 17**: Projected anomaly in mean wind speed (%) and direction for MAM (2051-2075 relative to 1981-2008) under the RCP8.5 pathway.*

In the MAM-season, the primarily southern direction in which winds blow over the Eastern Cape and Western Cape Provinces (Figure 4) are projected to deviate in a western direction in the RCP4.5 (Figure 16) and the RCP8.5 (Figure 17) pathways where current wind farm developments are underway. In the RCP4.5 pathway, winds are projected to deviate (Figure 16) minimally from their dominant directions (Figure 4) in central South Africa. However, in the western expanses of the country, the northerlies (Figure 4) are projected to deviate to an eastern direction (Figure 16). Winds in the Limpopo area are projected to remain fairly unchanged in the both the RCP4.5 (Figure 16) and RCP8.5 (Figure 17) pathways. North-westerlies along the Eastern Cape coast (Figure 4) are projected to deviate in the opposite direction i.e. to the southwest in both pathways (Figures 16 and 17).

The north-easterlies in Limpopo (Figure 6) are projected to deviate in a southern direction in both the RCP4.5 (Figure 18) and RCP8.5 (Figure 19) pathways in the JJA-season. The north-

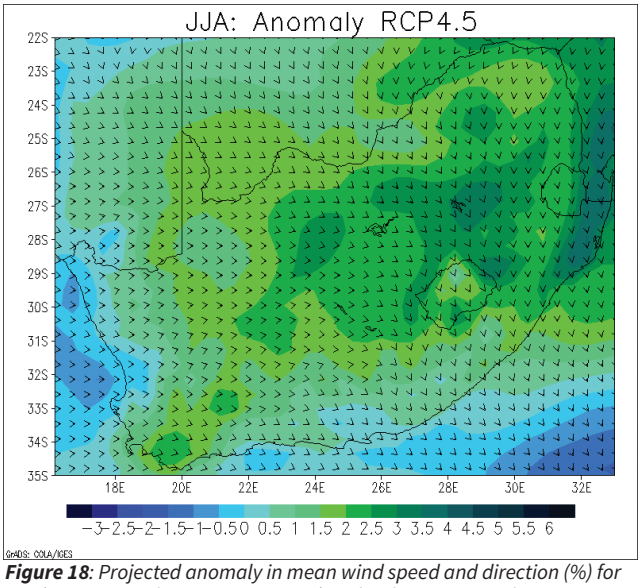

***Figure 18**: Projected anomaly in mean wind speed and direction (%) for JJA (2051-2075 relative to 1981-2005) under the RCP4.5 pathway.*

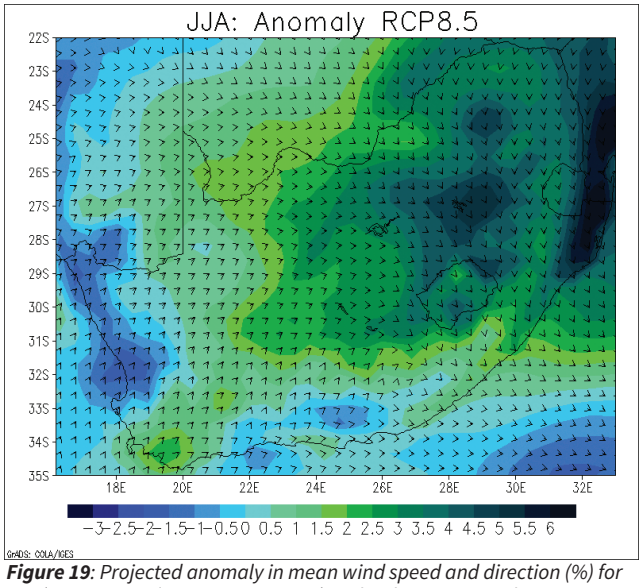

***Figure 19**: Projected anomaly in mean wind speed and direction (%) for JJA (2051-2075 relative to 1981-2005) under the RCP4.5 pathway.*

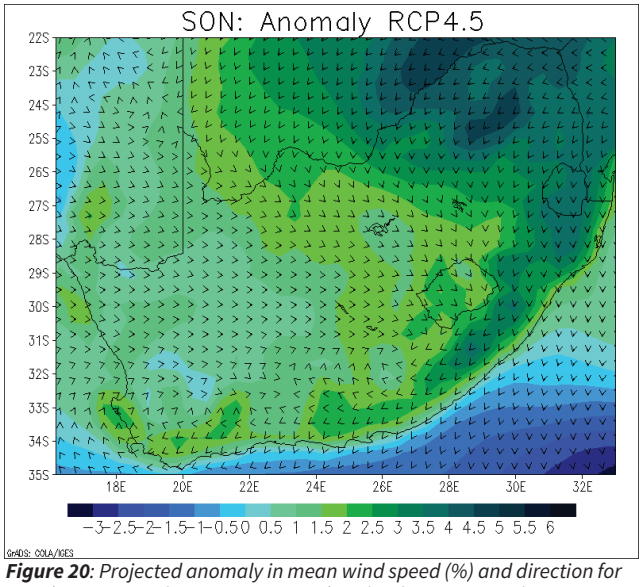

***Figure 20**: Projected anomaly in mean wind speed (%) and direction for SON (2051-2075 relative to 1981-2005) under the RCP4.5 pathway.*

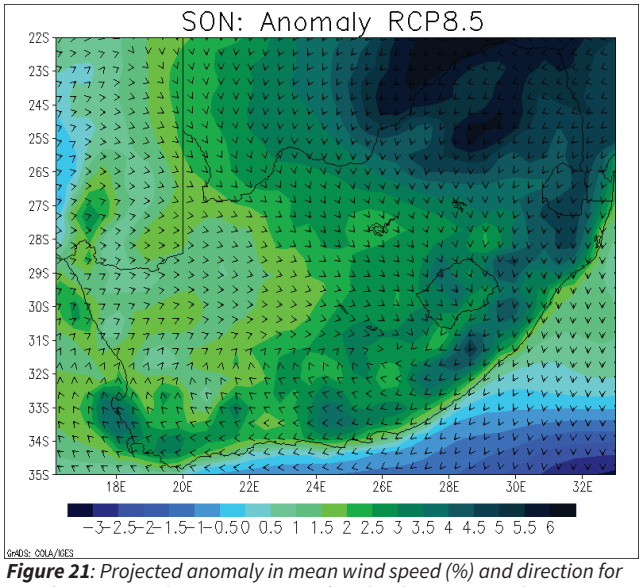

***Figure 21**: Projected anomaly in mean wind speed (%) and direction for SON (2051-2075 relative to 1981-2008) under the RCP8.5 pathway.*

westerlies over the Western Cape and Eastern Cape Provinces (Figure 6) are projected to deviate very little in the RCP4.5 pathway (Figure 18), but are projected to deviate in a northern direction under the RCP8.5 pathway (Figure 19).

While wind directions in the eastern half of the country (Figure 8) are projected to remain relatively unchanged in the SON-season under both the RCP4.5 (Figure 20) and RCP8.5 (Figure 21) pathways, they are projected to deviate to the west along the coasts of the Western Cape and Eastern Cape Provinces under both pathways (Figures 20 and 21). South-westerly winds in the Northern Cape Province (Figure 8) are projected to deviate in an eastern direction in both pathways (Figures 20 and 21).

Conclusions

Numerous studies are beginning to clarify the impacts of climate change on various physical climatic variables (Fant et al., 2015). Two such variables, wind speed and direction, were assessed in this study to gauge its potential changes in South Africa within the mid-21st century (2051-2075), relative to a historical period (1981-2005). Seasonal daily mean wind speed increases rarely reach 6% and decreases occur to a maximum of 3% and are variable between different seasons and areas within the country. In all seasons except DJF, wind speeds are projected to increase in the Highveld region, suggesting that air pollution dispersing conditions could increase. Dominant wind direction at the 850hPa level is projected to remain unchanged, except over the Western and Eastern Cape provinces in most seasons.

RCPs impact the severity of changes in wind speeds, showing that climate change mitigation measures could curb drastic changes to wind climates in South Africa (Fant et al., 2015). Climate change impact studies such as this one could also

contribute to understanding its potential effects on various other sectors such as wind energy (Herbst & Lalk, 2014). The findings of the study are consistent with those of Jury (2013). In his 20th century analysis, he found no trend in surface zonal winds, but future projections from circulation models suggested intensified easterly flow along the south coast of South Africa.

References

Bernard S.M., Samet J.M., Grambsch A., Ebi K.L. & Romieu I. 2001, 'The potential impacts of climate variability and change on air pollution-related health effects in the United States,' *Environmental Health Perspectives* 109:109-209.

Christensen O.B., Gutowksi W.J., Nikulin G. & Legutke S. 2014, CORDEX Archive Design. CORDEX Experiment Guidelines. Available: http://cordex.dmi.dk/joomla/images/CORDEX/cordex_archive_specifications.pdf [Date Accessed 15 July 2014].

CTEC 2015, Model evaluation methods. Available http://www.ctec.ufal.br/professor/crfj/Graduacao/MSH/Model%20evaluation%20methods.doc [Date Accessed 2 February 2015].

Dee D.P., Uppala S.M., Simmons A.J., Berrisford P., Poli P., Kobayashi S., Andrae U., Balmaseda M.A., Balsamo G., Bauer P., Bechtold P., Beljaars A.C.M., Van de Berg L., Bidlot J., Bormann N., Delsol C., Dragani R., Fuentes M., Geer A.J., Haimberger L., Healy S.B., Hersbach H., Hólm E.V., Isaksen L., Kållberg P., Köhler M., Matricardi M., McNally A.P., Monge-Sanz B.M., Morcrette J.-J., Park B.-K., Peubey C., De Rosnay P., Tavolato C., Thépaut J.-N. & Vitart F. 2011, 'The ERA-Interim reanalysis: configuration and performance of the data assimilation system,' *Quarterly Journal of the Royal Meteorological Society* 137:553-597.

Fant C., Schlosser C.A. & Strzepek K. 2015, 'The impact of climate change on wind and solar resources in southern Africa,' *Applied Energy*, Article in Press [Available from:http://dx.doi.org/10.1016/j.apenergy.2015.03.042].

Herbst L. & Lalk J. 2014, 'A case study of climate variability effects on wind resources in South Africa,' *Journal of Energy in Southern Africa* 25:2-10.

Horton D.E., Skinner C.B., Singh D. & Diffenbaugh N.S. 2014, 'Occurrence and persistence of future atmospheric stagnation events,' *Nature Climate Change* 4:698-703.

Jarvis C.H. & Stuart N. 2001, 'A Comparison among Strategies for Interpolating Maximum and Minimum Daily Air Temperatures. Part I: The Selection of ''Guiding'' Topographic and Land Cover Variables,' *Journal of Applied Meteorology* 40:1060-1074.

Jury M. 2013, 'Climate trends in southern Africa,' *South African Journal of Science* 109(1/2):11 pages.

Moss R.H., Edmonds J.A., Hibbard K.A., Manning M.R., Rose S.K., Van Vuuren D.P., Carter T.R., Emori S., Kainuma M., Kram T., Meehl G.A., Mitchell J.F.B., Nakicenovic N., Riahi K., Smith S.J., Stouffer R.J., Thomson A.M., Weyant J.P. & Wilbanks T.J. 2010. 'The next generation of scenarios for climate change research and assessment,' *Nature*, 463:747-756.

Pašičko R., Branković C. & Šimić Z. 2012, 'Assessment of climate change impacts on energy generation from renewable sources in Croatia,' *Renewable Energy* 46:224-231.

Rasmussen D.J., Holloway T. & Nemet G.F. 2011, 'Opportunities and challenges in assessing climate change impacts on wind energy - a critical comparison of wind speed projections in California,' *Environmental Research Letters* 6 [Available from: DOI 10.1088/1748-9326/6/2/024008].

Van Vuuren D.P., Edmonds J., Kainuma M., Riahi K., Thomson A., Hibbard, K., Hurtt G.C., Kram T., Krey V., Lamarque J., Masui T., Meinshausen M., Nakicenovic N., Smith S.J. & Rose S.K. 2011. 'The representative concentration pathways: an overview,' *Climatic Change* 109:5-31.

The use of fine water sprays to suppress fume emissions when casting ferromanganese

Sarel J. Gates*[1], Gerrit Kornelius[1], Steven C. Rencken[1], Neil M. Fagan[1], Peter Cowx[2], Luther Els[3]
[1]University of Pretoria, Dept of Chemical Engineering,Environmental Engineering Group,
Private Bag X20 Hatfield, Pretoria, South Africa, 0028, gerrit.kornelius@up.ac.za
[2]Eramet Norway, Sauda, Norway, peter.cowx@erametgroup.com
[3]Resonant Environmental Technologies, P.O. Box 12225, Centurion, South Africa, 0046, luther@resonant.co.za

Received: 14 October 2015 - **Reviewed:** 26 November 2015 - **Accepted:** 30 November 2015
http://dx.doi.org/10.17159/2410-972X/2015/v25n2a3

Abstract
During the casting of ferromanganese alloys from electric arc furnaces into sand beds at temperatures of up to 1800°C a considerable amount of very brown fumes are generated when the alloy fume is oxidized in the atmosphere. The fume is difficult to capture because of the large flux of gas that is generated. Possible reasons for this flux include the high evaporation rate of Mn at elevated temperatures, the large surface area of the casting beds and the large thermal plumes over the furnace tapholes and casting beds. It has been found that the use of fine water sprays along the edge of the roof that covers the casting bed resulted in a significant reduction in visible emissions. This paper describes research into the kinetics of the fume to improve the design of the capture hoods, as well as the mechanism of suppression by the water sprays by using CFD analysis. It is shown that the oxidation reaction produces less than 20% of the energy content of the plume over the arc furnace taphole, and also that radiation heat transfer may play an important role in increasing the energy content of the taphole plume. The capture of fume particles by fine spray droplets is shown to have limited efficiency, while the heat sink that is caused by evaporation does not materially contribute to the circulation of fume through the spray. It is postulated that the increased moisture content of the air over the casting beds may be instrumental in reducing the oxygen partial pressure or in the formation of an oxide layer, both of which would reduce metal evaporation and, therefore fume formation. The exact mechanism requires further investigation.

Keywords
ferromanganese, secondary fume, water sprays, fume capture hoods, fume extraction, ferro-alloy tapping

Introduction
Eramet Sauda, in Norway, operates two ferromanganese furnaces producing high carbon ferromanganese (HCFeMn) as well as a Manganese Oxygen Refining (MOR) unit to produce medium and low-carbon ferromanganese (LCFeMn). Secondary fume emissions occur at the tapholes of the arc furnaces as well as during post-taphole operations. The current secondary fume capturing system has good capacity, but emissions do still escape from the furnace building. Due to their small particle size, manganese oxides that are present in these fumes pass through the trachea and bronchi to the lungs (de Nevers 2010). Health risks include manganism, a serious and irreversible brain disease, and various lung disorders. It is therefore important to either suppress or capture the fumes formed during casting operations (Goodfellow et al. 2001). The formation mechanism of the fumes was investigated in order to understand its possible contribution to the fume emission volume and energy content. A study was then conducted to investigate whether a fine water spray can suppress fume emissions from casting bed operations and, consequently, mitigate Mn_3O_4 pollution without enclosing the sand beds or significantly increasing the fume capture capacity. To achieve this, flat jet sprayers were placed on the edge of the shed roof that cover the casting beds. These sprayers sprayed horizontally away from the shed to form a water curtain on the outside of the shed without water accumulation in the shed.

Theoretical Background

Fume Energy Contributions

Mechanisms and Fume Formation
Little information on the fume generation mechanisms in the ferromanganese industry could be found, but studies in other similar applications suggest that the predominant mechanisms in steelmaking are bubble bursting and volatilisation (Guézennec et al. 2004; Huber et al. 2000; Gonser et al. 2011). There is little bubble formation during the metal flow, from one casting pocket to the next. Due to the high metal temperatures and the low relative boiling point of Mn, evaporation and oxidation to Mn_3O_4 is considered the most significant mechanism of the fume generation. Mn_3O_4 has the highest Gibbs Free energy of the manganese oxides, making it the most likely product to form at

the elevated temperatures found during casting operations (Els et al. 2013).

The energy generated by the reaction involved in the Mn_3O_4 formation, can be assumed to contribute to the fume's energy. A discussion of the reaction kinetics involved in the Mn_3O_4 formation will help in the understanding of the unexpected high energy content of the fumes, the fumes' rise velocity and the necessary extraction required to ensure that the fumes are captured.

Lee et al. (2005) considered various reaction-limiting factors for the fume formation in the casting of the high carbon FeMn produced in the arc furnace. They found that the Mn in the melt is essentially lost through evaporation and oxidation to form MnO mist, which is further oxidised to Mn_3O_4 particulate. Turkdogan et al. (1963) studied the diffusion-limited rates of vaporization of metals and showed that at high oxygen partial pressures, metal evaporation rates approach those in a vacuum and can be predicted by the Langmuir equation:

$$E_a = p_a \left(\frac{M_a}{2\pi RT}\right)^{0.5} \quad (1)$$

where R is the gas constant, T the absolute temperature, E_a and M_a the evaporation rate and the molar mass of a respectively (Turkdogan et al. 1963; Dennis et al. 2001)[1]. This effect is known as oxidation enhanced vaporization and is caused by the oxidation of the metal vapour above the liquid surface (Turkdogan et al. 1963) to form the MnO mist, reducing the Mn concentration in the gas-liquid interface and promoting further evaporation of Mn into this sink.

In reality the O_2 concentrations may not be high enough to cause O_2 enhanced oxidation. Lee et al. (2005) suggest that no MnO mist and, therefore, no Mn_3O_4 forms when the O_2 partial pressure is below 17kPa, which may be the case where decarburisation of HCFeMn occurs during tapping.

The possible rate limiting factors are the mass transfer of Mn in the melt to the gas-liquid interface, evaporation of Mn at the interface, Mn vapour transport away from the interface and transport of O_2 to the interface. The high metal temperature ensures that the evaporation of Mn is fast. Because of the relative abundance of Mn in the melt, it is not likely to be depleted at the metal surface. Therefore the MnO fume formation rate is considered to be controlled by the counter-diffusion of Mn and O_2 in the boundary layer above the metal surface (Dushman et al. 1962), which can be expressed mathematically with:

$$J_{Mn} = J_{O_2} = \frac{h_{Mn}}{RT}\left(P_{Mn}^{sat} - p_{Mn}\right) \quad (2)$$

where J_{Mn} is the evaporation flux of the Mn, J_{O_2} the flux of O_2 to the gas-liquid interface, $h_{Mn} = D_{Mn}/l$ the average mass transfer coefficient of the Mn vapour and p_{Mn} the partial pressure of Mn at the top of the mass transfer boundary layer (l).

[1] Unless indicated otherwise, all equations are expressed in SI units

According to Lee et al. (2005), the affinity of O_2 with Fe (at high temperatures) is approximately two orders of magnitude less than that of Mn, rendering the formation of FeO negligible.

Radiation Effects

The net rate of radiation can be expressed with the following equation (Çengel et al. 2011; Welty et al. 2009):

$$Q = \sigma\varepsilon A_s T_s^4 - \sigma\alpha A_s T_{surr}^4 \quad (3)$$

where σ is the Stefan-Boltzmann constant ($5.67\times10^{-8}\ W/(m^2 \cdot K^4)$), ε the emissivity of the surface, A_s the surface area, α the absorptivity of the surface, T_s and T_{surr} the temperatures of the surface and surroundings, respectively.

Due to the significant difference between the temperature of the melt and its surroundings, the amount of energy released from the melt in the form of thermal radiation is high. The energy transfer rate varies between 100kW/m^2 and 300kW/m^2, depending on the metal's surface temperature and the emissivity. It is improbable that the melt will absorb a significant amount of energy (Els et al. 2013).

The generated fumes primarily consists of Mn_3O_4 particulates, which results in the hazy appearance. Non-polar gasses are virtually unaffected by radiation effects, whilst polar molecules are capable of absorbing radiation (Çengel et al. 2011; Modest 2003). With the above-mentioned in mind, the thermal radiation will be dependent on the Mn_3O_4 particulate content of the fumes. Energy may be reflected by the particulates and may further be re emitted. The exact effects of the particulate presence in the plume are at this stage difficult to quantify.

Natural Convectional Effects

As Els et al. (2010) describe, the majority of fume extraction systems are designed based on flow rates calculated from thermal updrafts which are caused by convection. The convective heat transfer rate is calculated by using *Equation* (4) (Çengel et al. 2011):

$$\Phi = hA_s(T_s - T_\infty) \quad (4)$$

where h is the convective heat transfer coefficient, A_s the surface area of the melt, T_s and T_∞ the surface temperature and surrounding air temperature respectively (Çengel et al. 2011).

Furthermore, there is also natural convective heat transfer between the air and the droplets from the water spray, where a spraying system is used.

Water Spray System

Overview

To attempt to reduce the amount of fugitive secondary fumes formed during casting of ferromanganese on casting beds, Els et al. (2014) studied the possibility of implementing air curtains, enlarging the extraction volume or extending the tapping

shed structure. As expected, the efficiency increases when the operational area is enclosed or the extraction volume is increased. Some of the experimental runs that use air curtains also show promising results. In an attempt to find a more efficient alternative, water sprays were installed at the casting beds at Eramet Sauda. The implementation of a water curtain was found to visibly reduce the fume concentration over the casting beds. Two mechanisms were thought to influence the secondary fume.

The first involves the suppression of fume emissions because of the water spray acting as a heat sink, which enhance convectional effects. The air density in the vicinity of the water droplets tends to increase as the air temperature decreases, resulting in buoyancy effects playing a role. The change in circulatory pattern and/or the increased humidity of the air is believed to be involved in the enhanced rate of formation of an oxide layer on the molten metal, thereby reducing the rate by which fumes form. This will be discussed further under *Heat Transfer Effects* on this page.

The second postulated effect of the water spray may comprise the mass transfer of Mn_3O_4 particles from the fumes to the water droplets. It is expected that the Mn_3O_4 particulates will be captured by the water droplets, and then settle on the floor. Thereafter appropriate processing actions may be taken to manage the Mn_3O_4 particles.

Computer Fluid Dynamics (CFD) Modelling

Due to the complex flow patterns of the fumes, a computational model is necessary to efficiently determine the air flow patterns (Witt et al. 2006). CFD modelling was therefore used to simulate the fumes rising off the casting beds and the effect of the water spray. The simulations were performed using FloEFD 14.1.0 (Mentor Graphics 2015). Figure 1 provides a CFD simulation of the temperature profile over a casting bed, where the water spray system (situated at the edge of the roof over the casting bed) is inactive. The CFD simulation delivered comparable results to the on-site measurements of the fugitive fumes' temperature. The air flow patterns of this base case were compared to the air flow patterns when the spray system was activated and the spray acted as a heat sink.

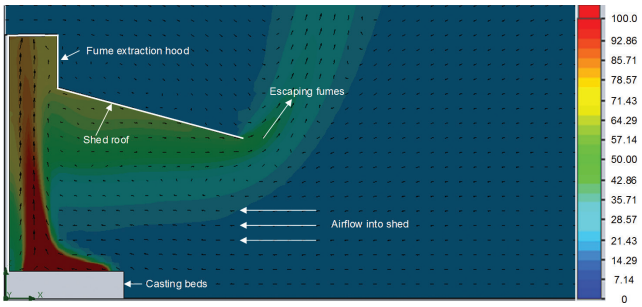

***Figure 1**: Base case CFD showing the temperature with the scale on the left.*

Spray Pattern Development

The amount of heat and mass transfer effects of the spray depends on the spray area. Spray area determination requires modelling of the droplet trajectory. Droplets were assumed to be homogenous in size and shape after dispersion from the spray. It is reasonable to assume that heat transfer effects will have the largest effect at the top of the shed where the highest temperature occurs. The initial horizontal velocity of the droplet can be determined by *Equation* (5):

$$v_d = \frac{Q_d}{A} \quad (5)$$

where v_d is the velocity Q_d the water volumetric flowrate and A the open area of the spray nozzle. Once dispersed, the horizontal velocity of the droplets decreases exponentially due to drag force effects. Two possible relationships between C_d and the Re_d are expressed in *Equations* (6) and (7) (de Nevers 2010):

$$C_d = \frac{24}{Re_d}, Re_d < 0.3 \quad (6)$$

$$C_d = \frac{24}{Re_d}(1 + 0.14R_d^{0.7}), 0.3 \leq Re_d \leq 1000 \quad (7)$$

where Re_d is the dimensionless Reynolds number which can be calculated with (Çengel et al. 2011):

$$Re_d = \frac{\rho D_d v_d}{\mu} \quad (8)$$

where ρ is the fluid density, D_d the droplet diameter and μ the fluid viscosity.

Since the decrease in the droplets' velocity is much greater than its decrease in the diameter, it is assumed that the droplet's diameter remains constant when the area of water dispersion is calculated. The horizontal velocity of the droplets was modelled in time increments of 0.1s until the horizontal component of the velocity has decreased to zero. This implies that only vertical forces are still active after this point.

For reasons of simplicity, it is assumed that the time it takes until the droplet is influenced only by vertical forces is negligible in comparison with the total falling time. For the transfer of particulate to the droplets, a homogenous dispersion of droplets is assumed to fall vertically from the roof height to the floor over the entire spray area. Finally, the spray area is calculated as the product of the shed roof length and the horizontal distance that the droplets travel.

Heat Transfer Effects

Balances:

By assuming that the heat which is transferred to the water is the same as the heat that is lost through hot air escaping from underneath the shed roof in a steady state operation, and that the kinetic and potential energies are negligible, the energy balance reduces to *Equation* (9):

$$\sum M_{in} C_{p_{in}} T_{in} = \sum M_{out} C_{p_{out}} T_{out} \quad (9)$$

where C_p is the specific heat capacity at constant pressure, M the mass, and T the absolute temperature.

Noting that the particulate concentration is low, the mass balance becomes:

$$M_{a_{in}} + M_{\mathcal{H}_{in}} + M_{w_{in}} = M_{a_{out}} + M_{\mathcal{H}_{out}} + M_{w_{in}} \quad (10)$$

where M_a, M_H and M_w represents the mass of dry air, water vapour in the air and water from the sprayers respectively.

Humidity

Absolute humidity is defined as the mass of water vapour per unit of dry air and can be expressed mathematically for an air-water system as in *Equation* (11) (Green et al. 2007):

$$\mathcal{H} = \frac{0.622 p_v}{P - p_v} \quad (11)$$

where p_v is the vapour pressure of water at a given temperature and P the total pressure of the air-water system. The evaporation rate of the water droplets is dependent on the humidity of the air.

Drop Diameter

It is further assumed that the water and air are at thermal equilibrium as it leaves the control volume. Therefore, the temperature of the water and air will be equal. According to Holterman (2003), a droplet's temperature will decrease as it falls through the air as a result of evaporation and will continue to decrease until the water reaches the wet-bulb temperature. The difference in temperature of the droplets and the air results in energy transfer, with the droplets acting as heat sinks. This transfer of heat may affect the droplet's diameter significantly. Various models describing the change in droplet diameter have been developed by Ranz et al. (1952), Goering et al. (1972) and by Williamson et al. (1974). Williamson (*ibid.*) proposed using *Equation* (12) to determine the change in droplet diameter:

$$\frac{dD_d}{dt} = -\frac{4MW_L D_{v,f}}{D_d \rho_d R T_f} \Delta p \left(1 + 0.276 R e_d^{\frac{1}{2}} Sc^{\frac{1}{3}}\right) \quad (12)$$

where MW_L is the molecular weight of the evaporating liquid, ρ_L the density of the drop, $D_{v,f}$ the average diffusion coefficient for the vapour molecules in the saturated film around the drop, T_f the average absolute temperature in the film, Re the Reynolds number, Sc the Schmidt's number, Δp the difference between the vapour pressure near the drop and at the ambient atmosphere and R the gas constant.

It is assumed that the heat transfer effects will result in the droplets to evaporate uniformly. Diffusivity dependence on temperature is given by *Equation* (13) (Welty et al. 2009):

$$D_{AB} \propto T^{\frac{3}{2}} \quad (13)$$

Schmidt's number is defined as (Çengel et al. 2011):

$$Sc = \frac{\mu_{a,f}}{\rho_{a,f} D_{v,f}} \quad (14)$$

where the subscript f indicates that the given properties is at the film temperature.

Mass Transfer Effects

Mass transfer occurs when Mn_3O_4 particulates come into contact with the water droplets. The droplet size as well as the particle characteristics influence the capture efficiency. Furthermore, the water curtain is dependent on the nozzle type (Grant et al. 2000; Nuyttens et al. 2007). Flat jet K 1590 type nozzles are installed at Eramet Sauda. The control volume for the material balance is illustrated in Figure 2, adapted from de Nevers (2010)

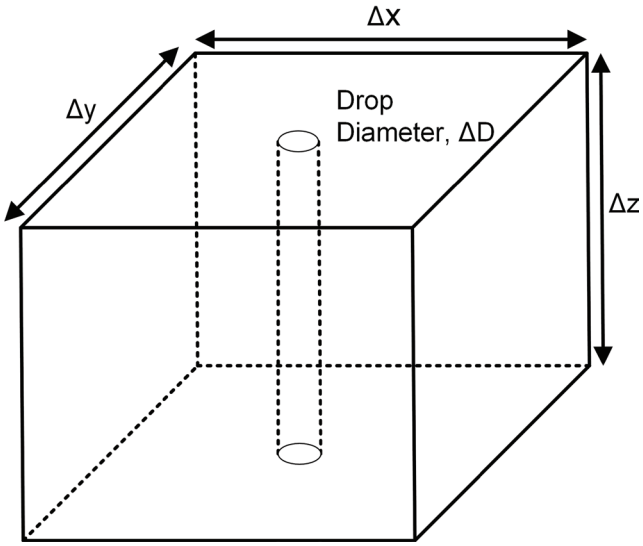

***Figure 2**: Control volume (de Nevers 2010)*

Particulate Distribution

A chemical analysis of the fumes showed that Mn_3O_4 formed about 97% of the total mass. The particle size distribution (PSD), shown in Figure 3, was measured by laser diffraction. The particles have a mean diameter of about 0.6µm.

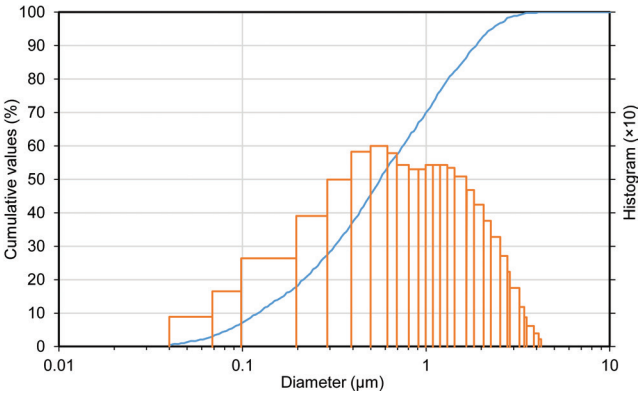

***Figure 3**: Particle size distribution for the fume*

Water Droplet Characteristics

It is assumed that for each Δz increment, the droplet characteristics remain constant in terms of diameter and droplet shape. Further assuming that the droplet is spherical, the volume through which the droplet falls can be calculated by

(de Nevers 2010):

$$V_{swept} = \frac{\pi}{4} D_d^2 \Delta z \quad (15)$$

where V_{swept} is the sweeping volume, D_d the droplet diameter and Δz the incremental length.

Assuming spherical droplets and uniform distribution of the fume particulate in the air, the efficiency of particle capture, as illustrated graphically in Figure 4 (Kopita 1955).

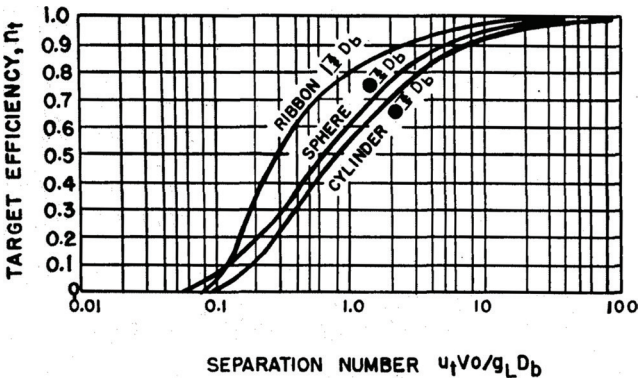

***Figure 4**: Target efficiency correlation (Kopita 1955)*

The separation number can be calculated with *Equation* (16) adapted from de Nevers (2010):

$$N_s = \frac{\rho_p D_p^2 v_{d,t}}{18 \mu_g D_d} \quad (16)$$

where D_p is the diameter of the particle, μ_g the viscosity of the plume and $v_{d,t}$ the terminal velocity of the droplets. Once the target efficiency is known, the mass of particles absorbed can be calculated with *Equation* (17) (de Nevers 2010):

$$M_{transfered} = \frac{\pi}{4} D_d^2 \Delta z c \eta_t \quad (17)$$

where c represent the particle concentration which can be calculated with *Equation* (18) (de Nevers 2010):

$$\frac{dc}{dt} = -\frac{1.5 c \eta_t Q_d}{D_d A} \quad (18)$$

where η_t is the target efficiency, Q_d the volumetric flowrate of the water droplets, D_d the droplet diameter and A the spray area.

The initial particle concentration is estimated as the concentration that is measured when the sprayer system is inactive. If the initial concentration is known, the above equation can be solved without difficulty. The remaining concentration is a function of time, which is determined by the water droplet's settling velocity. Because the droplets are small, they will rapidly reach their terminal settling velocity; the assumption is therefore made that the droplets reach terminal settling velocity at the edge of the shed roof.

Acting Forces on the Water Droplet

Considering the forces acting on the water droplets, Newton's second law of motion reduces to *Equation* (19) (de Nevers 2010).

$$ma = \rho_d \left(\frac{\pi}{6}\right) D_d^3 g - \rho_{fluid} \left(\frac{\pi}{6}\right) D_d^3 g - F_d \quad (19)$$

where m is the mass of a water droplet, a its acceleration, ρ_d its density, g the gravitational constant, ρ_{fluid} the density of the fluid (in this case air) through which the droplets falls and F_d the drag force. According to Çengel et al. (2011), the general equation for the relationship between the drag coefficient (C_D) and the drag force (F_d) is given by:

$$F_d = \frac{1}{2} C_D \rho_{fluid} v_d^2 A \quad (20)$$

where A represents the spray area, ρ_{fluid} the fluid density and v_d the droplet velocity. Together with the relationship between the Reynolds number and the drag coefficient for spherical droplets, this can be used to calculate the terminal velocity for each of the assumed droplet sizes. The effectiveness of the spray system can then be found from:

$$\eta_{overall} = \frac{c_0 - c}{c_0} \times 100 \quad (21)$$

Summary

To be able to design a more efficient extraction system, it is necessary to know the extent of fume formation and how energy contributors (heat of formation, radiation and natural convection) will effect these fumes. The Mn formation is suspected to be controlled by the diffusion of the Mn through the gas-liquid interface, although Lee et al. (2005) indicates that no Mn vapour will form if the oxygen partial pressure is below 17kPa.

Various attempts to reduce the secondary fumes have led to the conclusion that the fumes will be captured by increasing the extraction volume or designing a closed structure in which casting operations will occur. These solutions are however expensive. In an attempt to find a more efficient and cost effective solution, Eramet Sauda installed water sprayers. As a result fume emissions were visibly reduced.

Two possible mechanisms were investigated which may be influential in the water curtain's ability to visibly reduce secondary fumes over the casting beds. The first involved the heat transfer between the fumes and the water spray, which were affected by the energy content of the fumes, the humidity of the air and the change in the droplet's diameter. The second possible mechanism was the mass transfer of Mn_3O_4 particulates from the fume to the droplets, which were affected by the particle's and droplet's characteristics as well as the forces acting on the droplet. CFD simulations were used to model the effects of the reduction mechanisms on the air flow patterns and compare the obtained results with the base case where the water spray system was not used.

Results and Discussion

Plant Specific Information

The parameters shown in Table 1 are the characteristics of the spray system and environment.

***Table 1**: Parameters at Eramet Sauda*

Description	Value	Units
Total pressure	101.3	kPa
Hot air temperature	45	$°C$
Ambient temperature of the air	20	$°C$
Water temperature	12	$°C$
Relative humidity at ambient air temperature	70	%
Droplet diameter	250	μm
Height of shed roof	6	m
Sprayer spacing along the roof	2	m
Water flowrate out of the sprayers	15	L/min

Figure 5 provides a schematic representation of the shed and sprayer system.

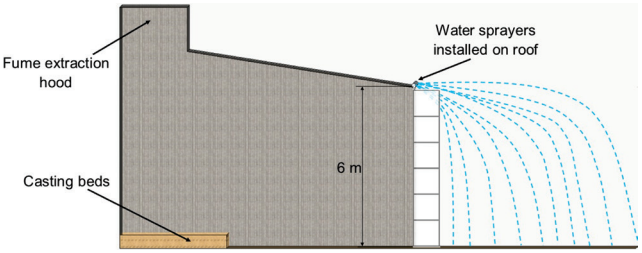

***Figure 5**: Schematic of shed and sprayers*

Note the 1m by 1m control volume blocks extending vertically beneath the sprayers. These will be discussed further in *Heat Transfer* on page 32.

Fume Formation

Previous CFD Modeling

Els et al. (2013) used CFD modelling to simulate fumes rising from the casting beds. Initially they only modelled the heat transfer from the metal and structural surfaces due to convection and radiation. They found that the amount of transferred heat was significantly lower than the energy measured on-site as discussed in the next paragraph. They adjusted the model to include additional heat transfer. Figure 6 (Els et al. 2013) illustrates the results from the verification model and Figure 6 depicts the velocity plot of the fumes from the outside of the shed that covers the entire casting bed area.

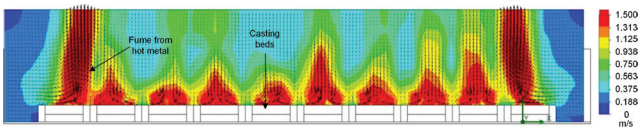

***Figure 6**: Verification model velocity plot (Els et al. 2013)*

Previous Flowtests

Table 2 provides the data that Els et al. (2013) found from on-site measurements. They showed from the comparison of theoretical calculated values and the measured data that the energy released as a results of the formation of the Mn_3O_4 fumes produced about 20% of the total fume energy. Some additional fume energy may be attributed to radiation effects which may play an important role in the fumes' energy content.

***Table 2**: Previous test results (Els et al. 2013)*

Test Point	MOR fan	LCFeMn pour point	Units
Velocity	36.5	32.6	m/s
Temperature	20.1	35.8	$°C$
Static pressure	-3.57	-2.57	kPa
Volume flow	48.5 156861	43.3 134513	Am^3/s Nm^3/h
Mass flow	58.1	49.3	kg/s
Energy	-	2.5	MW

Previous Conclusions

By using the model described above, Els et al. (2013) proved that a 100% fume removal efficiency will require either the extraction volume to be doubled or that the beds should be entirely enclosed. This would have been expensive and the spray system mechanisms (as explained in the following sections) were therefore developed. The spray system's role in visible fume reduction was investigated for the purpose of using this knowledge in future spray model designs. This investigation included air flow patterns, heat transfer and mass transfer of the particulates to the water droplets from the spray.

Air Flow Over the Casting Beds

Water disperses up to 8m outwards from the shed, and as a CFD input, this was broken down into 1m sections with temperature decreasing linearly over the 8m distance. The CFD is simulated with a length along the roof edge of 3m, exposing a $3m^2$ surface area for air flow from under the roof edge into the first control volume as seen in Figure 7.

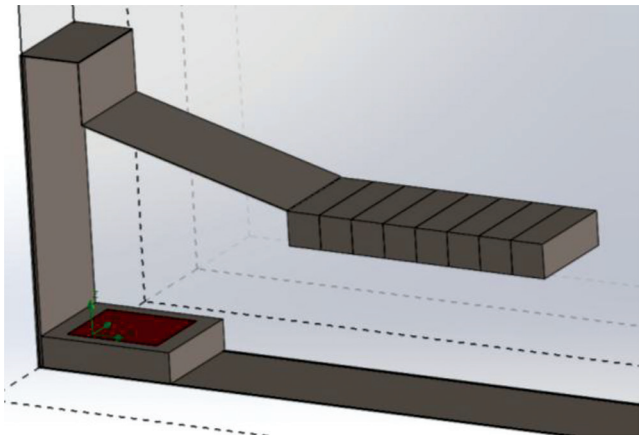

***Figure 7**: 3D representation of the model*

The heat sink was assumed to occur in this control volume. Since the heat sink will have an influence on the circulation pattern (i.e. the flow rate outward from under the roof edge and hence the outward velocity of the air), a trial and error approach

was applied to find the air flowrate into the heat sink. Firstly, the heat sink values for a number of assumed air flow rates were determined using the energy balance described in *Heat Transfer Effects* on page 28. These heat sink values were used as input parameters for the CFD simulations and a velocity profile was determined. By comparing the assumed air flow rates to the resulting CFD output, the approximate velocity of the air could be determined. The calculated heat sink values based on different air inlet flowrates are displayed in Table 3.

***Table 3**: Heat sink results from the energy balance over the control volume*

Description	Values			Units
Air flow rate	3.00	4.00	5.00	(m^3/s)
Air velocity	1.00	1.33	1.67	(m/s)
Block 1	8.90	11.7	14.5	(kW)
Block 2	7.99	10.5	13.0	(kW)
Block 3	7.05	9.25	11.5	(kW)
Block 4	6.10	7.99	9.87	(kW)
Block 5	5.12	6.70	8.27	(kW)
Block 6	4.12	5.38	6.64	(kW)
Block 7	3.10	4.04	4.97	(kW)
Block 8	2.06	2.66	3.26	(kW)

The CFD simulations using the heat sinks in Table 3 are shown in Figure 12, Appendix A. Comparing the CFD results and the calculations explained in Table 3, the air flow rate outwards from under the shed roof was determined to be roughly 4m^3/s for the 3m length of roof modelled.

Heat Transfer

Overview

The heat transfer was modelled in two stages: the first involved using a control volume approach for the first (top) section shown in Figure 5, whilst the second involved using an incremental time approach for the rest of the sections in Figure 5.

First Section

Using the air flow rate as determined in *Air Flow Over the Casting Beds* on page 31, the amount of water that evaporated was calculated and the results appear in Table 4.

***Table 4**: Results after top meter heat transfer*

Description	Value	Units
Hot air temperature	45	$°C$
Relative humidity at hot air temperature	24.4	%
Ambient temperature of air	20	$°C$
Water temperature	12	$°C$
Total heat sink	58.2	kW
Total water mass in	0.375	kg
Total mass evaporated	0.020357	kg
Mass of water out	0.0204	kg
Initial droplet diameter	250	μm
Droplet diameter leaving control volume	245	μm
Average temperature out (T_f)	19.73	$°C$

Lower Section

The air temperature varies slightly from the second meter to the floor, with the air mainly at a temperature of around 20°C and the water temperature at 19.73°C. At 20°C the air is approximately 70% humid and the total driving force for heat transfer is small. This implies that the air will not necessarily reach saturation and the control volume approach would be inaccurate, therefore an incremental time approach would be preferred.

Using *Equation* (12) at incremental steps of 0.01s, the droplet depletion rate is calculated for the remaining 5m (lower) section. This gives the droplet size as well as the mass of water that evaporated after each meter that the droplet falls vertically. The results are displayed in Table 5. From the change in the droplet diameter per meter shown in Table 5, one realises that the change in droplet diameter can be regarded as negligible. Therefore a constant diameter of 245.33µm was used for the mass transfer calculations in the control volumes below the first (upper) one.

Using the approach described above, it was shown (see Appendix A) that the inward air velocity under the edge of the roof increased somewhat with the introduction of the sprays, and that the air flowing over the casting beds will originate from the area where the moisture content is being increased by the water sprays.

***Table 5**: Results for the lower section*

Sections	Mass evaporated (kg)	New drop diameter (μm)
2nd meter	8.0973E-06	245.327
3rd meter	8.2443E-06	245.324
4th meter	8.2441E-06	245.321
5th meter	8.2439E-06	245.319
6th meter	8.2437E-06	245.316

Transfer of Particles to Droplets

The capture efficiency was calculated by considering the relationship in Figure 4 between the capture efficiency and the separation number. *Equation* (16) was used to determine the separation number. The capture efficiency was calculated to be zero. This calculation is validated by de Nevers (2010, 302), who states that for particles less than 1µm the efficiency tends to be zero.

Calculations were done to determine the efficiency of droplet sizes equal to 250µm for different particle sizes given that the inlet flow rate of 15L.min^{-1} was used. The graph in Figure 8 (in effect Figure 4 on an extended scale) shows that for particles

between 0.9µm and 3µm, which are easily inhaled, the capture is negligible.

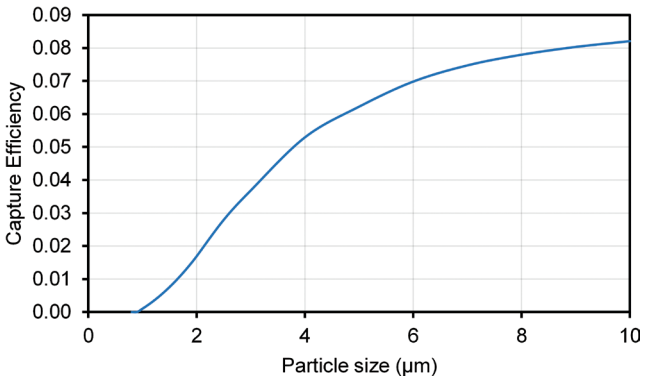

***Figure 8**: Capture efficiency for small particles*

Since the PSD (Figure 3) shows a large number of very fine particles, an investigation was done on smaller droplet sizes and their capture efficiency. The graph in Figure 9 shows the capture efficiency of the small particle sizes at different droplet sizes.

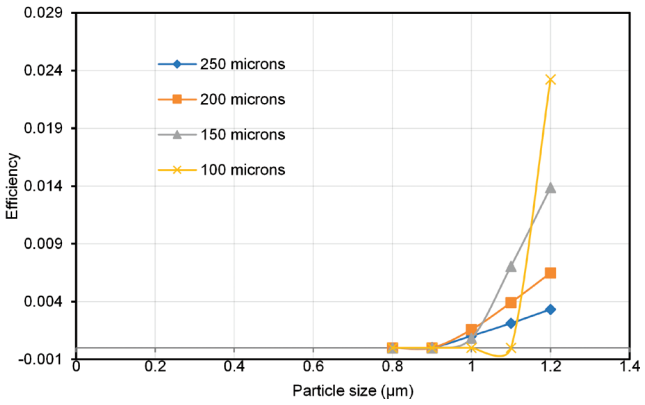

***Figure 9**: Captured efficiency variation with droplet size*

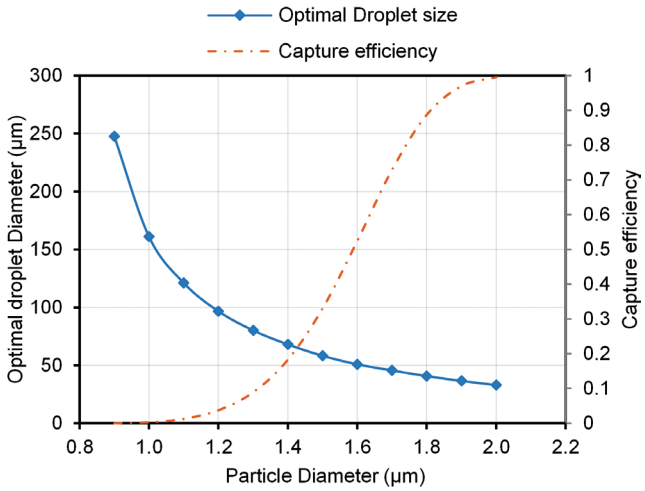

***Figure 10**: Capture efficiency for optimal droplet diameter*

For particles less than 0.8µm, no droplet size showed any capture efficiency. Droplet sizes of 200µm and 250µm captured a small quantity of particles between 0.9µm and 1µm. This is verified by de Nevers (2010, 292), who also suggests that small particles have a tendency to follow a stream line around the object, thereby not easily captured by small droplets.

The calculation procedure was repeated in an attempt to find an optimum droplet size for capture of the critical particle size. The optimal diameter that would result in the largest capture efficiency is shown in Figure 10.

Conclusions

To fully understand the fine water spray system's role in suppressing secondary emission fumes, it is necessary to understand the mechanism involved in the formation of these fumes, as well as possible energy contributors to the fumes' energy content. Considering this, a previous investigation was reflected upon, which involved a combination of heat transfer relationships and CFD modelling to determine possible energy contributors as well as possibilities for better extraction. It was shown that the oxidation reaction involved during the fumes' formation contributed only 20% of the fumes' energy. Based on these plume energy determinations it was found that a 100% fume removal efficiency from the casting shed was possible if either the extraction volume was increased or if the shed was completely enclosed. Unfortunately these solutions are expensive.

A fine water spray system was considered as an alternative solution. After the installation of the spray system a reduction in the amount of visible fume was noticed. Before the installation of the spray system, a slight circulation pattern was observed, which was further enhanced by the spray system. This phenomenon was investigated by considering the heat transfer between the water and the fume-containing air escaping from under the roof. The investigation showed that the heat transfer is most significant near the shed roof and that the main effect was a slight increase in the inward velocity of the air flowing over the casting bed.

Another possible reduction mechanism that was investigated was the transfer of particulates to the water droplets. However, it was found that the capture efficiency tends to zero as a result of the small Mn_3O_4 particulates. Droplet sizes that are about 200µm are able to capture 1µm particles better than smaller droplets, however still at a very low efficiency. Particles that are smaller than 0.8µm will most likely remain suspended in the air.

It is believed that a spray system will work very well for particles larger than 1.4µm. Operations that have fumes containing particles of this magnitude will be able to use a sprayer system as an effective and cheap fume suppressing technique. For operations that contain a large majority of particles between 1µm and 1.5µm, it is recommended that two separate sprayers should be used. The one sprayer should disperse droplets between 200µm and 300µm, while the second sprayer should disperse smaller droplets.

A fine mist sprayer was installed directly over the casting beds

as shown in Figure 11 ensuring a more intense dispersion of moisture. It is clear that the fume concentration is dramatically decreased over the spray area. This leads the authors to believe that the increase in moisture content of the air over the beds – such as when a sprayer system is used – is instrumental in the formation of an oxide layer on the liquid metal, reducing metal vaporisation and thus fume formation. To optimise the sprayer system, further work is necessary to determine the mechanism of fume formation as well as the role of the water spray system to reduce the visible fume emissions.

***Figure 11**: Fine mist sprayers installed at bed top surface level*

References

Çengel Y.A., Ghajar A.J. & Ma H. 2011. Heat and Mass Transfer: *Fundamentals & Applications*, 4th ed., McGraw-Hill.

de Nevers N. 2010. *Air pollution control engineering*. Waveland Press.

Dennis J.H., Hewitt P.J., Redding C.A. & Workman A.D. 2001. A model for prediction of fume formation rate in gas metal arc welding (GMAW), globular and spray modes, DC electrode positive. *Annals of Occupational Hygiene*, 45, 105-113.

Dushman S., Lafferty J.M. & Brown S.C. 1962. Scientific foundations of vacuum technique. *American Journal of Physics*, 30, 612-612.

Els L., Coetzee C. & Vorster O. 'Design of tapping fume extraction systems for ferroalloy furnaces', *Twelfth International Ferroalloy Congress, Helsinki, Finland*, 2010. 6-9.

Els L., Cowx P., Kadkhodabeigi M., Kornelius G., Andrew N., Smith P. & Rencken S. 'Analysis of a ferromanganese secondary fume extraction system to improve design methodologies', *Thirteenth International Ferroalloy Congress, Almaty, Kazakhstan*, 2013. 9-13.

Els L., Cowx P., Smith P. & Nordhagen R. 2014. Analysis and optimization of fume extraction from a ferromanganese furnace tapping operation.
Goering C., Bode L. & Gebhardt M. 1972. Mathematical modeling of spray droplet deceleration and evaporation.

Gonser M. & Hogan T. 2011. *Arc welding health effects, fume formation mechanisms, and characterization methods*. INTECH Open Access Publisher.

Goodfellow H.D. & Tähti E. 2001. *Industrial ventilation design guidebook*. Academic press.

Grant G., Brenton J. & Drysdale D. 2000. Fire suppression by water sprays. *Progress in energy and combustion science*, 26, 79-130.

Green D. & Perry R. 2007. *Perry's Chemical Engineers' Handbook, Eighth Edition*. McGraw-Hill Education.

Guézennec A.-G., Huber J.-C., Patisson F., Sessiecq P., Birat J.-P. & Ablitzer D. 2004. Dust formation by bubble-burst phenomenon at the surface of a liquid steel bath. *ISIJ international*, 44, 1328-1333.

Holterman H. 2003. *Kinetics and evaporation of water drops in air*. IMAG Wageningen.

Huber J., Rocabois P., Faral M., Birat J., Patisson F. & Ablitzer D. 'The formation of EAF dust', *58th Electric Furnace Conference and 17th Process Technology Conference*, 2000. 171-181.

Kopita R. 1955. The Use of an Impingement Baffle Scrubber in Gas Cleaning and Absorption. *Air Repair*, 4, 219-232.

Lee Y.E. & Kolbeinsen L. 2005. Kinetics of oxygen refining process for ferromanganese alloys. *ISIJ international*, 45, 1282-1290.

Mentor Graphics 2015. FloEFD FE 14.1.0.

Modest M.F. 2003. *Radiative Heat Transfer, 2nd Edition*, 2nd ed. Burlington, Academic Press.

Nuyttens D., Baetens K., De Schampheleire M. & Sonck B. 2007. Effect of nozzle type, size and pressure on spray droplet characteristics. *Biosystems Engineering*, 97, 333-345.

Ranz W. & Marshall W. 1952. Evaporation from drops. *Chem. Eng. Prog*, 48, 141-146.

Turkdogan E., Grieveson P. & Darken L. 1963. Enhancement of diffusion-limited rates of vaporization of metals. *The Journal of Physical Chemistry*, 67, 1647-1654.

Welty J.R., Wicks C.E., Rorrer G. & Wilson R.E. 2009. *Fundamentals of momentum, heat, and mass transfer*. John Wiley & Sons.

Williamson R.E. & Threadgill E. 1974. simulation for dynamics of evaporating spray droplets in a gricultural spraying. *Trans ASAE Gen Ed Am Soc Agric Eng*.

Witt P., Solnordal C., Mittoni L., Finn S. & Pluta J. 2006. Optimising the design of fume extraction hoods using a combination of engineering and CFD modelling. *Applied mathematical modelling*, 30, 1167-1179.

Appendix A

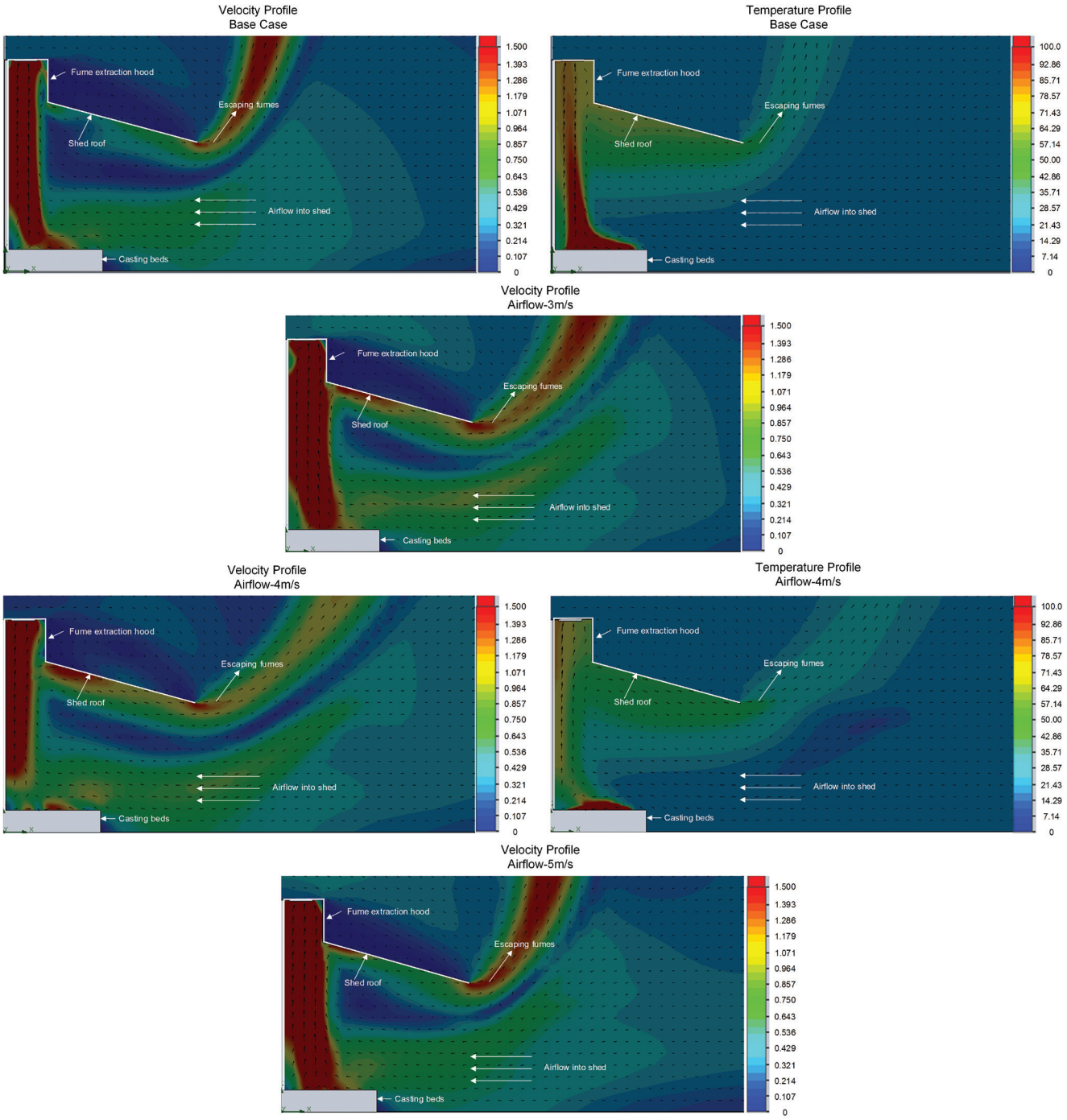

***Figure 12**: CFD results showing the airflow in the casting shed*

Quality Assurance of Continuous Emission Monitoring Systems: A practitioner's guide/technical report

Gerald Woollatt[1]

[1]LEVEGO, PO Box 422, Modderfontein, Gauteng, 1645, South Africa, Email: info@levego.co.za, Phone: 011 608 4148 Fax: 011 608 2621

Received: September 2015 - **Reviewed:** October 2015 - **Accepted:** October 2015

http://dx.doi.org/10.17159/2410-972X/2015/v25n2a4

Abstract

In 2004, the National Environmental Management Act (NEMA) and regulations were promulgated and by 2010 were gazetted into law for the first time in South Africa. Under the NEMA, the Air Quality Act 39 of 2004 (AQA) was promulgated and included priority pollutants identified by the Department of Environmental Affairs (DEA) as having or may have a significant detrimental effect on the environment, including health, social conditions, economic conditions, ecological conditions or cultural heritage. In this context continuous emission monitoring of emissions to air is a requirement under many of the operators as Air Emission Licenses (AEL) issued under section 21 of AQA. The quality of data obtained from continuous emission monitors is ensured by the inclusion of the BS EN14181:2004 (revised standard updated to current BS EN14181:2014) European standard which has been adopted into the South African legislation for this purpose.With this in mind the purpose of this technical paper is to provide an overview of the current status of automated measuring systems (AMS)/continuous emission monitors(CEMs) currently in use by industry to monitor emissions in South Africa, in terms of compliance with relevant emission limit values (ELVs) and the current challenges faced with ensuring the quality and reliability of the data obtained.

Keywords

CEMS/AMS, EN14181, TGN-M20, QAL1, 2 and 3

Introduction

In South Africa, there are currently no "South African" standards that have been developed for monitoring emissions to air. Instead the regulator has opted to adopt international best practise by utilising internationally recognised methods for air emissions monitoring and sampling.

Methods that have been adopted:

- European Committee for Standardization (CEN)
  - European EN Standards
- Environmental Protection Agency
  - USEPA Methods
- British Standards Institute (BSI)
  - British Standards
- International Standards Organization (ISO)
  - ISO Methods

Although these methods and standards have been adopted and widely utilised internationally the wholesale adoption of the standards without due consideration for the South African context is naïve and not without problems when it comes to the practical implementation of the standards or methods locally. It is for this reason that it is recommended that a review of the methods currently being utilised be conducted to ensure their relevance and applicability to the South African context.

One of the major shortcomings of the current legislation is the lack of a hierarchy of appropriate methods as per the United Kingdom Environment Agency Technical Guidance Note (TGN) M2 "Monitoring of stack emissions to air" This TGN describes the UK Environment agencies overall approach to stack-emission monitoring and provides guidance on methods used for regulatory purposes. It focuses on areas where practical guidance is necessary. This includes:

- The legislative framework
- The role of MCERTS (UK monitoring certification scheme for stack emission monitoring)
- Different approaches to stack emission monitoring
- Sampling strategy
- The hierarchy of different methods
- An index of monitoring methods

South Africa is currently in the unfortunate position that it has adopted many internationally recognized methods for sampling without any supplementary documentation with relevant practical guidance tailored to the South African context. The regulator will need to develop similar guidance as discussed here if it wishes to ensure quality and consistency of emission reporting throughout the country and across the industry as a whole.

When it comes to applying BS EN14181 the UK Environment agency has development TGN M20 "Quality assurance of continuous emission monitoring systems –application of EN14181 and BS EN 13284-2". The primary role of this technical guidance note is to provide guidance on the application of European standard "BS EN14181:2014, Stationary source emissions – Quality assurance of automated measuring systems".

It is important to note that the above standard utilises the term automated measuring systems (AMS) instead of continuous emission monitors (CEMs) however the terms are interchangeable and refer to the same concept. The guide summarizes the requirements of BS EN14181 and BS EN 13284-2 and provides guidance on how to perform each of the required tasks. It is important to remember that the TGN should always be read in conjunction with these standards and the relevant method implementation documentation. The development of equivalent South African TGN documents is therefore critical to ensure proper guidance and implementation is carried out where required.

Regulatory framework and standards for monitoring

It is important to note that up until June 2015 the BS EN14181 standard was applicable to all plants that fell under the European directives for the incineration of waste (WID) and large combustion plants (LCPD). Since June this year these two directives have been replaced by the Integrated Emission Directive (IED). Why is this important? It is important to note that these standards are not developed in a vacuum and supporting documentation such as the directives mentioned above are critical in assessing the applicability of methods and emission limit values etc. For example the monitoring of emissions to air for plants that fall under one of the directives need to be conducted according to the requirements of CEN, ISO or BS standards or applicable alternative method.

The TGN M2 document contains a table of approved methods with a hierarchy of methods that are applicable. In addition to the index of monitoring methods the directives specify the requirements for monitoring accuracy and precision through 95% confidence intervals. South Africa does not currently have any equivalent document. This needs to be developed in order to ensure that BS EN 14181 can be practically implemented in its entirety, without such guidance is a near impossible feat without adopting directives from other countries.

Scope and structure of BS EN14181

BS EN 14181 applies only to CEMs used for compliance monitoring and permanently installed IED installations. It does not apply to portable CEMs units or installations outside of the directives. South Africa needs its own similar directives for its industrial processes in order to ensure the correct applicability of EN14181. EN14181 specifies three quality assurance levels (QALs) and an annual surveillance test (AST) referred to as QAL1, QAL2, QAL3 and AST respectively (Figure 1).

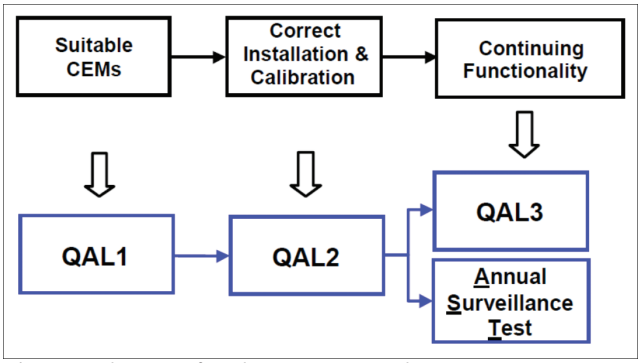

***Figure 1**: Schematic of Quality Assurance Levels*

QAL 1 – Specifies a procedure to demonstrate that the CEM is suitable for the intended purpose before installation, by meeting the required performance standards and the uncertainty allowances specified by the IED. This is difficult to demonstrate in South Africa without an equivalent directive being formally developed or adopted.

The first level of quality demonstrates the potential suitability of the CEM before it is installed on a stack. In England and Wales MCERTS product certification at an appropriate certification range is taken as evidence of compliance with the QAL 1 requirements. CEMs must meet certain performance requirements evaluated under the UK Environmental Agency's monitoring certification scheme MCERTS. Once the CEM has been installed the unit must have means for tests for linearity, zero and span drift and leak checking the entire system. The IED also specifies uncertainty allowances expressed as 95% confidence intervals. Table 1 details Baseline Ranges, ELV's and uncertainties.

Criteria in determining the suitability of CEMs:

- CEMs to be MCERTS certified for the determinants specified
- CEMs to be certified for the range it is to be utilised for
- Operator to ensure that the specific plant conditions will not reduce the performance of the CEM
- All CEMs must have provision that allow for zero, span and linearity checks to be performed
- Certification range is the lowest range over which MCERTS requirements are met
- The range would typically be set at a value at least twice the half hourly ELV of the intended application.

QAL 2 – Specifies a procedure to calibrate the CEM once it has been installed using standard reference methods (SRMs) and then verifying the required uncertainty allowances once installed. It is important to note that South Africa has not established its own uncertainty allowances as required by the standard or applicable directive.

The CEM instrument is calibrated using SRM parallel

***Table 1**: Selection of daily average ELV's including certification ranges and allowable uncertainties*

	ELV, $mg.m^3$	Certification range, $mg.m^{-3}$	Allowable uncertainty, %	Allowable uncertainty, $mg.m^{-3}$
NOx – incineration	200	300	20%	40
NOx – large combustion plant, solid/liquid fuel	200 - 600	500 - 1500	20%	40 – 120
NOx – large combustion plant, gaseous fuels	200 - 300	500 - 750	20%	40 – 60
NOx – large combustion plant, gas turbines	50 - 120	125 - 300	20%	10 – 24
SO_2 – large combustion plant, solid/liquid fuel	200 - 850	500 - 2125	20%	40 – 170
SO_2 – large combustion plant, gaseous fuels	35-800	88 - 2000	20%	7 – 160
SO_2 – incineration	50	75	20%	10
CO – incineration	50	75	10%	5
HCl – incineration	10	15	40%	4
Particulate matter, large combustion plant	30 - 50	75 - 125	30%	9 - 15
Particulate matter, incineration	10	15	30%	3
Particulate matter, co-incineration	30	45	30%	9
Total organic carbon, incineration	10	15	30%	3

measurements. The data obtained can then be utilised to calculate a calibration function for the CEM and determine it suitability for the specific application. The uncertainty for the CEM is then determined by calculating the variability of the calibration function.

It is important to note that the effectiveness of this test requires at least fifteen valid repetitions of each applicable SRM, over a three day period.

QAL 2 procedures are carried out when:

- Upon initial CEM installation
- At least every three to five years as per applicable directive
- Whenever there is a significant change in the plant operation which will have a change in the emissions
- After a failure of a CEM unit
- After a significant upgrade or other significant change to plant operations

QAL 3 – Specifies a procedure that ensures that the CEM remains within the required specifications during continued use. Drift and precision parameters are measured regularly by the plant operator. This data is then plotted utilising control charts such as CUSUM charts. The output of these charts will then determine the frequency of the CEM maintenance needed.

AST – The annual surveillance test is regarded as a mini QAL 2 test. The main objective of which is to determine whether the calibration function determined during QAL 2 tests is still valid. Functional tests need to be carried out. Once these have been conducted 3 – 5 parallel SRM measurements are conducted. If the AST shows the calibration is no longer valid then a full QAL 2 is required.

Calibration and Validation of the CEM according to QAL 2

The plant operators have the following responsibilities under QAL 2 to ensure valid data is obtained on a continual basis for reporting purposes:

- ensure the CEM is installed in the correcti location

Operators should follow the provisions for location and access described in TGN M1 and the method implementation document (MID) for EN15259 in order to determine the most representative location for the CEM according to the homogeneity test described in EN15259. The MID for EN15259 describes a procedure to determine whether the sample location will be representative or not. Grid measurements of the stack gas are conducted at centres of equal area across the sampling plane and comparing the results to a fixed reference point within the sampling plane.

- ensure sufficient access to the CEM to allow for regular maintenance, access and control of the unit
- ensure that the CEM is calibrated and operating correctly on a continual basis

To ensure that the CEMs are calibrated and operating correctly the following tasks need to be carried out. A set of functional tests and checks to ensure that the CEM has been installed correctly and is functioning at or better than the required performance levels required. A set of repeated parallel measurements to verify whether the readings from the CEM are reliable and to derive a calibration function if the SRM data shows that there is a bias in the CEMs readings. A set of statistical operations and tests following the parallel reference tests are conducted in order to verify whether the CEM meets the uncertainty budget as set out in the relevant directive. In Figures 2 and 3 the location of equal area points and sampling ports are shown. Figures 4 and 5 show examples of unsuitable and suitable sampling locations, respectively.

The test laboratory shall have overall responsibility for the functional tests, the checks may however be carried out by the operator, CEMs supplier or test laboratory and shall include the following checks, these checks are carried out prior to the parallel SRM measurements being conducted:

- Alignment and cleanliness
- Sampling system integrity
- Leak test
- Manual zero
- Span check
- Linearity
- Interferences
- Response time

EN14181 requires SRMs to be used to verify and calibrate CEMs. It is based on the following three premises for its effectiveness and accuracy. These are:

- There is a spread of data over the required range of the monitoring system
- There is a linear relationship between the CEM data and the SRM data when both sets of measurements are valid
- The SRM is linear, accurate and precise with an uncertainty no greater than half the maximum permissible uncertainty specified by the regulator.

Although EN14181 works best when there is good spread of data and the CEM has a linear response to increasing values of the target determinant, it is also common for emission results to be clustered, the most common patterns of emissions that test laboratories encounter are: linear (Figure 6), high level cluster (Figure 7) and low level cluster (Figure 8).

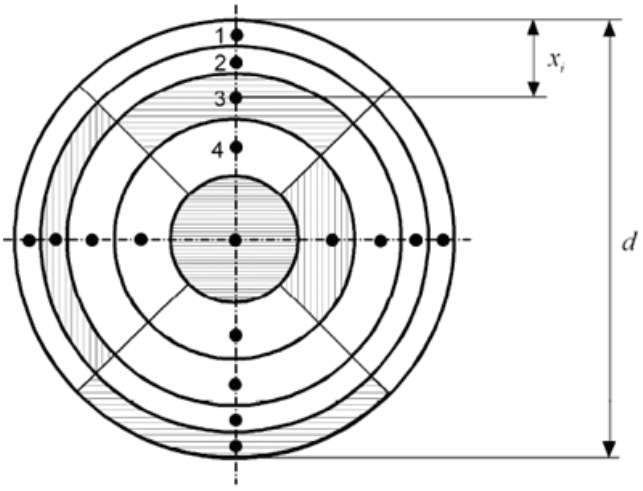

Figure D.1 — Sampling point positions in circular ducts - General method
(showing positions for ducts over 2 m in diameter –
The shaded positions are of equal area)

***Figure 2**: Location of equal area points*

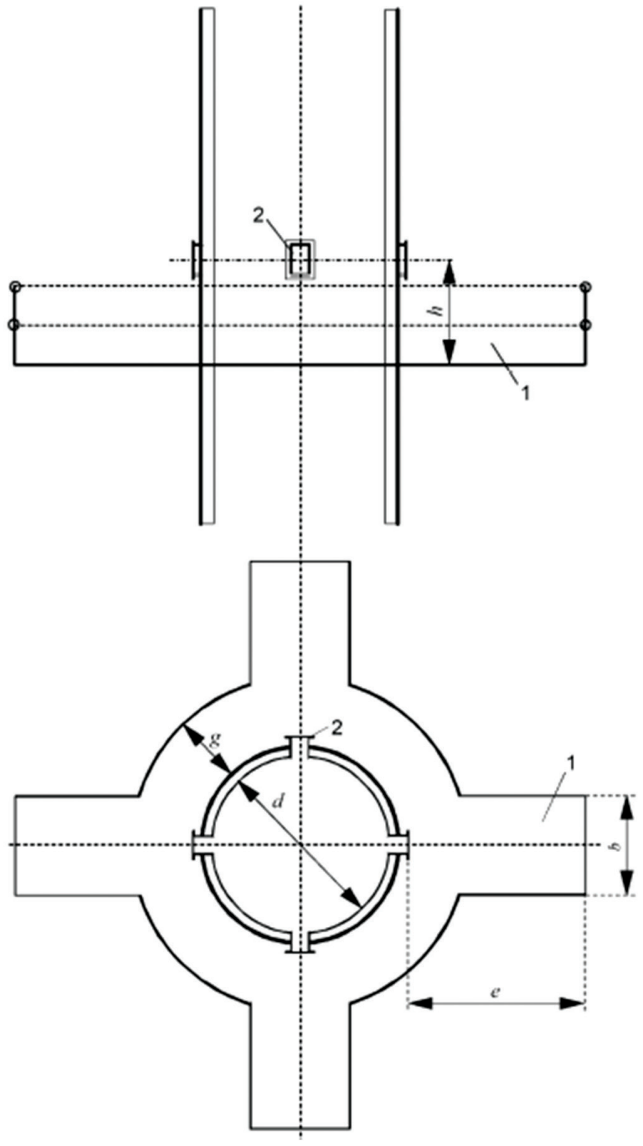

***Figure 3**: Location of the sampling ports*

***Figure 4**: Example of an unsuitable sampling location*

***Figure 5**: Example of a suitable sampling location*

It is important to note that if the emissions are typically below 30% of the ELV then EN13284-2 for low level particulate monitoring CEMs allows for the number of parallel measurements to be reduced from at least 15 measurements to three or five sets of parallel measurements. For the AST parallel measurements from at least five, to three to five repetitions. The total time of the measurement set should be at least 7.5 hours, however in certain circumstances such as batch process operations the times may be reduced in consultation with the operator and regulator justifying the request for reduced sampling.

Parallel measurements conducted for CEMs calibration purposes shall be performed with the CEMs and SRM in order to calibrate and validate the CEMs by use of an independent method e.g. BS EN13284-1. It is important to note that it is not sufficient to use reference materials alone to obtain the calibration function and this is therefore not permitted. Reference materials do not replicate sufficiently the matrix stack gas.

However, surrogate reference materials may be utilised to extend the valid calibration range of the CEMs which is typically 10% above the highest value measured with the SRM during the QAL 2 calibration procedure. It is also important to note that all test houses/labs conducting SRM tests must be accredited to EN14181 in addition to ISO 17025 accreditation for the applicable test methods.

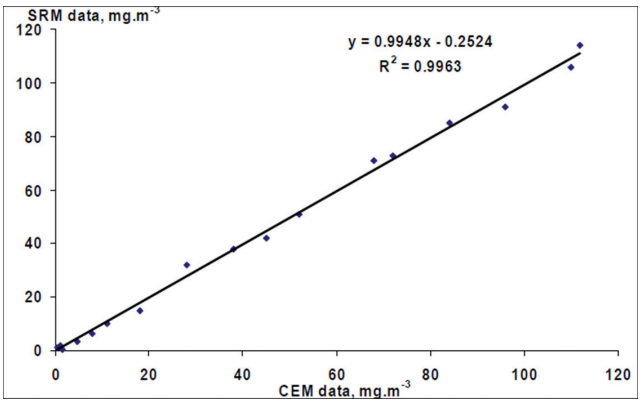

***Figure 6**: A linear spread of data across a wide range*

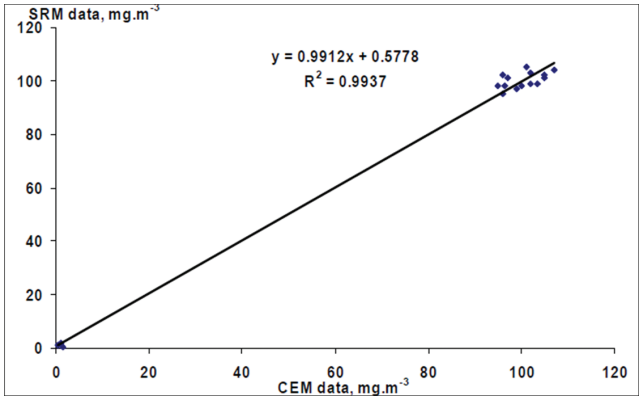

***Figure 7**: A high level cluster*

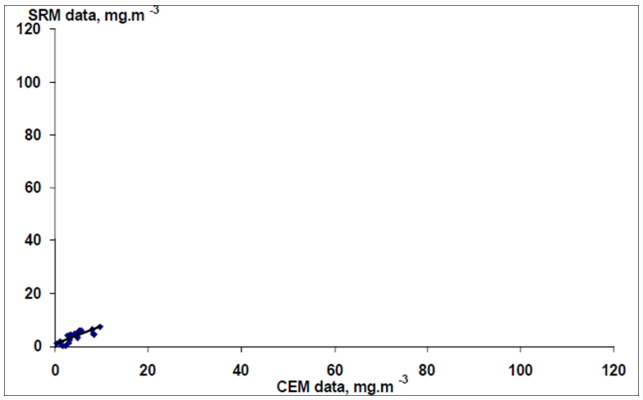

***Figure 8**: A low level cluster*

Key points for parallel measurements include:

- Only test houses accredited to ISO17025 for the MCERTS performance standards for manual stack monitoring for the applicable SRM's may perform the reference monitoring tests in QAL 2 and AST
- The applicable SRM's are prescribed in TGN M2
- The SRM data should have a wide spread over the measurement range, a low scatter and show a linear response
- The calibration function within QAL 2 and the AST is based on the premise that the SRM is sufficiently accurate and precise, as well as producing an adequate spread of data over the applicable range.

The calibration function is given by the following equation below:

$$\hat{y}_i = \hat{a} + \hat{b}\,x_i$$

where

$\hat{y}_i$ is the calibrated value of the AMS

x_i is the AMS measured signal

Each measured signal X_i of the CEMs shall be converted to a calibration signal value Y_i by means of the above calibration function. Once the calibration function has been established then a test for variability needs to be conducted the following steps are required:

- Tabulate the CEM and SRM data;
- Express the raw SRM data in the same conditions as the CEM data(i.e. either dry or wet and standard temperature and pressure;
- Plot the CEM and SRM data together;
- Assess whether there are any outliers;
- Calculate the calibration function – a valid calibration function is a correlation coefficient of the linear regression line of R^2 =0.9 or more;
- Establish the calibration range (should cover the ELV).
- Convert the data to calibrated and standardised values;
- Carry out the variability test; and
- Apply the calibration function.

Figure 9 shows the linear regression and derived calibration function for the Table 2 data set. The data set returns a correlation coefficient >=0.90%. This particular data set also passed the test for variability and therefore the derived calibration function calculated from the linear regression can be applied to the applicable CEM.

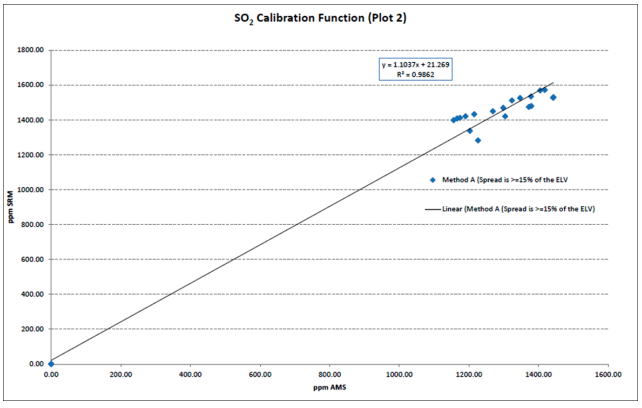

***Figure 9**: Linear regression and derived calibration function for the table 2 data set*

Actual emissions data

Table 2 present a data set obtained from a CEMs calibration survey conducted at a typical coal fired power plant in South Africa according to EN14181.

***Table 2**: Data set obtained from a CEMs calibration survey conducted at a typical coal fired power plant in South Africa.*

Component SO_2

Table: Raw measurements for the QAL2 test

		Sample Number	AMS Signal	SRM Value			
		i	x_i	y_i	*Difference* $D_i = y_{i,n} - \hat{y}_{i,n}$	*Difference* $Di - \bar{D}$	*Squared Difference* $(Di - \bar{D})^2$
Date	Time		ppm	ppm			
2014/10/02	19:00	1	1304.38	1420.05	115.67	-22.11	488.80
2014/10/02	20:00	2	1379.22	1478.81	99.59	-38.19	1458.50
2014/10/02	21:00	3	1441.97	1526.46	84.50	-53.29	2839.51
2014/10/02	22:00	4	1442.91	1529.62	86.71	-51.07	2608.59
2014/10/02	23:00	5	1372.25	1473.96	101.71	-36.07	1301.34
2014/10/03	02:00	6	1268.86	1448.79	179.93	42.15	1776.27
2014/10/03	03:00	7	1298.68	1468.96	170.28	32.50	1056.17
2014/10/03	04:00	8	1378.33	1533.92	155.58	17.80	316.74
2014/10/03	05:00	9	1417.93	1571.47	153.54	15.75	248.15
2014/10/03	06:00	10	1404.94	1568.21	163.27	25.49	649.51
2014/10/03	07:00	11	1347.18	1524.70	177.52	39.74	1579.06
2014/10/03	08:00	12	1323.65	1511.40	187.75	49.96	2496.27
2014/10/03	15:00	13	1155.96	1397.74	241.78	103.99	10814.63
2014/10/03	16:00	14	1166.14	1407.69	241.55	103.77	10767.76
2014/10/03	17:00	15	1174.55	1411.44	236.89	99.11	9822.08
2014/10/03	18:00	16	1190.08	1419.92	229.85	92.06	8475.64
2014/10/03	19:00	17	1215.37	1432.07	216.71	78.92	6228.94
2014/10/03	20:00	18	1202.93	1336.22	133.29	-4.49	20.16
2014/10/03	21:00	19	1226.35	1281.48	55.13	-82.66	6832.40
		20	0.00	0.00	0.00	-137.78	18984.36
		21	0.00	0.00	0.00	-137.78	18984.36
		22	0.00	0.00	0.00	-137.78	18984.36
		Sum			3031.24		126733.60
		Ave			137.78		
		SD					77.68

Conclusion

Considering the relative importance of obtaining reliable data to ensure legal compliance the correct implementation of EN14181 is critical.

Key points in addressing practical implementation of EN14181:

- It is recommended that South Africa develop or adopt its own technical guidance notes to address practical implementation of the standard applicable to the South African context.
- Test houses/laboratories in South Africa need to be accredited to ISO17025 to ensure data quality.
- Certification of personnel in South Africa equivalent to the UK Environment Agencies MCERTS scheme would be beneficial.
- Hierarchy of methods need to be established.
- Guidance from the regulator needs to be formalised to address the shortcomings in the legislation.
- Uncertainty and performance standards and requirements need to be established for ELV's and CEMs.

Establishing common reporting criteria with the help and guidance of the regulator with clear minimum requirements will help to standardise reporting allowing for proper permit compliance to be determined.

Acknowledgments

The author would like to thank the client who has so kindly allowed the use of their calibration data.

References

European Standard BS EN 14181, (2014). Stationary source emissions – Quality assurance of automated measuring systems.

European Standard BS EN 15259, (2007). Air quality – Measurement of stationary source emissions – Requirements for measurement sections and sites and for the measurement objective, plan and report

European Standard BS EN 13284-1, (2002). Stationary source emissions – Determination of low range mass concentration of dust – Part 1: Manual gravimetric method.

European Standard BS EN 13284-2, (2004). Stationary source emissions – Determination of low range mass concentration of dust – Part 2: Automated measuring systems.

International Organization for Standardization international standard ISO/IEC 17025, (2005). General requirements for the competence of testing and calibration laboratories (Edition 2).

Method Implementation Document for EN 15259, (2012). BS EN 15259:2007 Stationary source emissions – Requirements for the measurement sections and sites and for the measurement objective, plan and report.

Technical Guidance Note M1, (2010). Sampling requirements for stack emission monitoring, Environment Agency (Version 6)

Technical Guidance Note M2, (2011). Monitoring of stack emissions to air, Environment Agency (Version 8.1).

Technical Guidance Note M20, (2015). Quality assurance of continuous emission monitoring systems – application of EN14181 and BS EN13284-2, Environment Agency (Version 3)

Technical Guidance Note M21, (2010). Stationary source emissions – A procedure to use an Alternative Method for measuring emission of Sulphur dioxide, using instrumental techniques, Environment Agency (Version 1.1).